Available online at www.sciencedirect.com
ScienceDirect
Geochimica et Cosmochimica Acta 74 (2010) 661–683
Geochimica et Cosmochimica Acta
www.elsevier.com/locate/gca

Formation of pyroxenite layers in the Totalp ultramafic massif (Swiss Alps) – Insights from highly siderophile elements and Os isotopes

David van Acken [a,b,*], Harry Becker [a], Richard J. Walker [b], William F. McDonough [b], Frank Wombacher [a], Richard D. Ash [b], Phil M. Piccoli [b]

[a] *Freie Universität Berlin, Institut für Geologische Wissenschaften, AB Geochemie, Malteserstr. 74–100, Haus B, D-12249 Berlin, Germany*
[b] *Department of Geology, University of Maryland, College Park, MD 20742, USA*

Received 11 February 2009; accepted in revised form 1 October 2009; available online 7 October 2009

Abstract

Pyroxenitic layers are a minor constituent of ultramafic mantle massifs, but are considered important for basalt generation and mantle refertilization. Mafic spinel websterite and garnet–spinel clinopyroxenite layers within Jurassic ocean floor peridotites from the Totalp ultramafic massif (eastern Swiss Alps) were analyzed for their highly siderophile element (HSE) and Os isotope composition.

Aluminum-poor pyroxenites (websterites) display chondritic to suprachondritic initial γ_{Os} (160 Ma) of −2 to +27. Osmium, Ir and Ru abundances are depleted in websterites relative to the associated peridotites and to mantle lherzolites worldwide, but relative abundances (Os/Ir, Ru/Ir) are similar. Conversely, Pt/Ir, Pd/Ir and Re/Ir are elevated.

Aluminum-rich pyroxenites (clinopyroxenites) are characterized by highly radiogenic $^{187}Os/^{188}Os$ with initial γ_{Os} (160 Ma) between +20 and +1700. Their HSE composition is similar to that of basalts, as they are more depleted in Os, Ir and Ru compared to Totalp websterites, along with even higher Pt/Ir, Pd/Ir and Re/Ir. The data are most consistent with multiple episodes of reaction of mafic pyroxenite precursor melts with surrounding peridotites, with the highest degree of interaction recorded in the websterites, which typically occur in direct contact to peridotites. Clinopyroxenites, in contrast, represent melt-dominated systems, which retained the precursor melt characteristics to a large extent. The melts may have been derived from a sublithospheric mantle source with high Pd/Ir, Pt/Ir and Re/Os, coupled with highly radiogenic $^{187}Os/^{188}Os$ compositions. Modeling indicates that partial melting of subducted, old oceanic crust in the asthenosphere could be a possible source for such melts.

Pentlandite and godlevskite are identified in both types of pyroxenites as the predominant sulfide minerals and HSE carriers. Heterogeneous HSE abundances within these sulfide grains likely reflect subsolidus processes. In contrast, large grain-to-grain variations, and correlated variations of HSE ratios, indicate chemical disequilibrium under high-temperature conditions. This likely reflects multiple events of melt–rock interaction and sulfide precipitation. Notably, sulfides from the same thick section for the pyroxenites may display both residual-peridotite and melt-like HSE signatures. Because Totalp pyroxenites are enriched in Pt and Re, and depleted in Os, they will develop excess radiogenic ^{187}Os and ^{186}Os, compared to ambient mantle. These enrichments, however, do not possess the requisite Pt–Re–Os composition to account for the coupled suprachondritic ^{186}Os–^{187}Os signatures observed in some Hawaiian picrites, Gorgona komatiites, or the Siberian plume.

* Corresponding author. Present address: NASA/Lyndon B. Johnson Space Center, 2101 NASA Parkway, MS KR, B31, Houston, TX 77058, USA. Tel.: +1 2812446723.
E-mail address: david.vanacken@nasa.gov (D. van Acken).

0016-7037/$ - see front matter © 2009 Elsevier Ltd. All rights reserved.
doi:10.1016/j.gca.2009.10.007

1. INTRODUCTION

Clinopyroxenites and websterites occur as layers or dykes in peridotite massifs, mantle tectonites associated with ophiolites, and mantle xenoliths. They comprise about 1–5% of peridotite massifs (e.g. Kornprobst, 1969; Pearson and Nowell, 2004; Downes, 2007), but are rarely found in association with abyssal peridotites (Dantas et al., 2007). Past studies have suggested that pyroxenite layers in the mantle may play an important role during the genesis of basaltic magmas at mid-ocean ridges (Hirschmann and Stolper, 1996) and intra-plate settings (Lassiter et al., 2000; Hirschmann et al., 2003; Sobolev et al., 2005). In order to estimate the influence pyroxenites may have on basalt genesis and upper mantle refertilization, the formation of pyroxenite layers must be better understood.

A number of processes might lead to the formation of pyroxenites in the mantle, including: (a) formation as tectonically emplaced slices of subducted eclogitic crust, or residues of in situ partial melting of such eclogites (Polvé and Allègre, 1980; Loubet and Allègre, 1982; Allègre and Turcotte, 1986; Blichert-Toft et al., 1999; Morishita et al., 2003; Obata et al., 2006), (b) crystal accumulation at high pressures from asthenosphere-derived magmas passing through the lithosphere (Obata, 1980; Irving, 1980; Sinigoi et al., 1983; Bodinier et al., 1987, 1990; Takahashi, 1992; Vaselli et al., 1995; Becker, 1996; Kumar et al., 1996; Garrido and Bodinier, 1999), whereby the magmas may be derived from partial melting of subducted crust (Davies et al., 1993; Pearson et al., 1993), (c) in situ metamorphic segregation of pyroxene from the host peridotite (Dick and Sinton, 1979) or in situ crystallization of partial melts from peridotite wall rock (Sinigoi et al., 1983; Voshage et al., 1988), (d) melt–rock reaction between existing pyroxenite, host peridotite and percolating melt (Garrido and Bodinier, 1999), or reaction of melt derived from subducted eclogitic oceanic crust with peridotite in the asthenosphere (Yaxley and Green, 1998).

Pyroxenites and associated peridotites often show evidence for a depleted mantle origin. Depletion of light rare earth elements (REE), compared to heavy REE, is commonly seen in both pyroxenites and associated peridotites (Bodinier et al., 1987; Bodinier, 1988; Garrido and Bodinier, 1999; Bodinier and Godard, 2003). Initial ratios of $^{87}Sr/^{86}Sr$ and $^{143}Nd/^{144}Nd$ show considerable variation, and overlap with data for mantle peridotites, forming a cluster in the depleted mantle field (e.g. Voshage et al., 1988; Downes et al., 1991; Mukasa et al., 1991; Pearson et al., 1993; Downes, 2007). Because of these broad similarities, lithophile incompatible trace elements and isotope systems may provide only limited information about pyroxenite formation processes. Highly siderophile elements (HSE; including Os, Ir, Ru, Pt, Pd and Re) and the long-lived Re–Os isotope system, however, provide a different perspective on pyroxenite formation. Under upper mantle conditions, these elements mostly show chalcophile behavior and a wide range of compatibility during mantle melting. While Os, Ir and Ru are considered compatible during partial mantle melting in the presence of sulfides, Pt and Pd can behave compatibly as well as incompatibly, whereas Re is moderately incompatible (Morgan and Lovering, 1967; Morgan et al., 1981; Roy-Barman and Allègre, 1994). Peridotites as mantle residues often show depletion in Pt, Pd and Re (e.g. Pearson et al., 2004; Luguet et al., 2007), whereas mantle melts, represented by basalts, are enriched in those elements compared to the more compatible Os, Ir and Ru (Rehkämper et al., 1999a; Bézos et al., 2005; Dale et al., 2008).

Because of the large difference in partitioning behavior between Os and Re, partial melts with high Re/Os develop radiogenic $^{187}Os/^{188}Os$ over time, while mantle residues often display unradiogenic $^{187}Os/^{188}Os$. The large differences in Os isotopic composition and HSE signatures between melts and residues allow the use of HSE for the study of pyroxenite formation and melt–rock interaction in the Earth's mantle.

Field and petrographic observations from the Jurassic Totalp massif, eastern Switzerland, combined with major element, Sm–Nd and Re–Os isotopic data for the host peridotites provide evidence for refertilization of the host spinel lherzolites by melts related to the pyroxenite layers (Peters and Stettler, 1987; Müntener et al., 2004; van Acken et al., 2008). Refertilization of the massif may have occurred in the spinel lherzolite–spinel–garnet pyroxenite facies of the former oceanic lithosphere beneath the Tethys ocean basin in a regime, transitional between lithosphere and asthenosphere. In the present study, abundances of Os, Ir, Ru, Pt, Pd and Re and Os isotope compositions from websterite and clinopyroxenite samples of the Totalp massif were obtained, to constrain melt–rock interaction, pyroxenite formation and the origin of the infiltrating mafic melts.

2. GEOLOGY AND PETROLOGY

The Totalp ultramafic massif in eastern Switzerland consists of serpentinized spinel lherzolites associated with layered and folded spinel and spinel–garnet clinopyroxenites, spinel websterites, and more rarely spinel orthopyroxenites. The massif forms part of the Arosa imbricate zone, which separates the Penninic and Austroalpine units (e.g. Schmid et al., 2004). It was emplaced on the ocean floor of the Jurassic Piedmont-Liguria branch of the Tethys Ocean. The Piedmont-Liguria ocean basin underwent a period of spreading from 210 to 160 Ma and attained a maximum width of ~500 km (Stampfli and Borel, 2004; Schmid et al., 2004). For a detailed geological overview and a geological map see, for example, Desmurs et al. (2002) and Schmid et al. (2004); for paleogeographical reconstructions see Manatschal and Bernoulli (1998) and Stampfli and Borel (2004).

The Totalp ultramafic massif has been tectonically overturned, but is in primary contact with radiolarites and ophicalcitic breccias (Weissert and Bernoulli, 1985). From $^{39}Ar/^{40}Ar$ dating of phlogopite from pyroxenites, a formation age of the body of 160 Ma has been inferred (Peters and Stettler, 1987). U–Pb ages of 160 ± 1 Ma from zircons in oceanic gabbro from the nearby Platta locality (Schaltegger et al., 2002) suggest coeval magmatism, and thus, proximity to an ocean ridge environment at the time of emplacement.

Biostratigraphic correlation of overlying concordant sediments suggests emplacement at the ocean floor at approximately the same time (Weissert and Bernoulli, 1985). The presence of spinel in the lherzolites, and spinel and spinel–garnet assemblages in the pyroxenites combined with the absence of plagioclase in both lithologies indicate that the last equilibration occurred in the deeper lithospheric mantle, followed by rapid uplift. Equilibration temperatures between 830 and 975 °C, and a pressure of 10 ± 3 kbar were estimated for a last equilibration under spinel lherzolite facies conditions (Peters and Stettler, 1987).

During the Alpine orogeny, the ultramafic body was obducted along with surrounding sediments and basaltic and gabbroic rocks (Peters and Stettler, 1987; Müntener et al., 2004; Stampfli and Borel, 2004). The pyroxenites are sometimes folded and concordant, or oblique to a high-temperature foliation (Peters, 1963), and occasionally show well-preserved igneous textures (Peters, 1963, 1968; Peters and Stettler, 1987). Extensive melt–peridotite interaction during episodes of melt migration has been suggested (Müntener et al., 2004; Piccardo et al., 2004; van Acken et al., 2008). Following Jurassic seafloor alteration and serpentinization, the rocks underwent a very low grade metamorphic overprint in the course of the Alpine orogeny, with peak temperatures of about 100–150 °C (Früh-Green et al., 1990).

Several hypotheses regarding the magmatic and tectonic history of the Totalp massif have been proposed: (a) emplacement in a fracture zone (Weissert and Bernoulli, 1985), (b) magmatic formation at an ultraslow-spreading ocean ridge (Lagabrielle and Lemoine, 1997) similar to the modern day Southwest Indian or Arctic Gakkel ridges (Dick et al., 2003; Michael et al., 2003) and (c) origin in the subcontinental mantle and emplacement on the ocean floor during late stages of continental rifting (Peters and Stettler, 1987; Müntener and Hermann, 2001; Desmurs et al., 2002; Müntener et al., 2004).

3. METHODS

Sixteen websterites, spinel- and spinel–garnet pyroxenites from pyroxenitic layers from the Totalp massif were studied for major element compositions, HSE concentrations (Re, Os, Ir, Ru, Pt and Pd) and Os isotopic composition. Several samples were collected in association with adjacent peridotites or comprise profiles across modally layered pyroxenites. Layer thickness varies from few mm up to ca. 0.5 m. Detailed descriptions of Totalp pyroxenite samples from this study are given in the Electronic annex.

3.1. Whole rock analyses

Some layered pyroxenites were cut using a diamond blade. The cut surfaces were abraded, using sand paper or sintered corundum in order to remove possible contamination from saw marks. Most samples were first disintegrated into chips using a ceramic jaw crusher. For some samples (TA11, TA13, TA61) a Mn steel jaw crusher was used. After cleaning with ultrapure water, sample chips were powdered in an agate disk mill.

Whole rock major element abundances, H_2O and C contents were determined using XRF, Karl-Fischer titration and IR-based CSA at Universität Karlsruhe (CSA302; Leybold Heräus; for details, see Becker, 1996) and GFZ Potsdam (LECO RC-412-Analyzer (H_2O, CO_2). Reproducibilities (2σ) are 2–3% for SiO_2, MgO and FeO, 5–8% for Al_2O_3, and CaO and 10–20% for Na_2O, TiO_2 and MnO. Accuracy was monitored using ultramafic rock standards (DTS-1, UB-N, PCC-1) that were included with each batch of samples and yielded results within quoted precisions. Sulfur concentrations were determined at the University of Leicester, using a LECO CS 230 Carbon/Sulfur Determinator.

For the determination of HSE abundances and Os isotope analysis, between two and three grams of sample powder were spiked with mixed ^{99}Ru–^{105}Pd–^{191}Ir–^{194}Pt– and ^{185}Re–^{190}Os spikes prior to digestion. Digestion was performed using 2.5 ml conc. HCl and 5 ml conc. HNO_3 in sealed borosilicate glass Carius tubes at 220 °C for 24 h followed by high-pressure digestion at 320–345 °C for 48 h, using the technique outlined in Becker et al. (2006).

Osmium separation and analysis followed a modified procedure of Cohen and Waters (1996). After opening of the Carius tubes, Os was extracted from the acid phase into CCl_4, and then extracted back into HBr. A microdistillation technique (Birck et al., 1997) was used to further purify the Os fraction. After microdistillation, the sample Os was loaded in HBr onto baked Pt filaments (99.995% ESPI) and covered with NaOH–$Ba(OH)_2$ activator solution.

Osmium isotopic ratios were measured as OsO_3^- using negative thermal ionization mass spectrometry (N-TIMS) at the Freie Universität Berlin (FUB), using a ThermoFinnigan Triton instrument, and at the University of Maryland (UMD) using a VG Sector-54 and a NBS-designed single collector thermal ionization mass spectrometer. Signals were detected on Faraday cups in static mode or by SEM in pulse counting mode, depending on signal intensity. All measured ratios were corrected for interferences from isobaric OsO_3^- molecules: oxygen isotope corrections were made using $^{18}O/^{16}O$ and $^{17}O/^{16}O$ of 0.00204 and 0.00037, respectively. Measured ratios were mass fractionation corrected to a $^{192}Os/^{188}Os$ ratio of 3.08271 (Shirey and Walker, 1998) using the exponential fractionation law. For the low-Os samples, $^{187}Os/^{188}Os$ was corrected for spike contribution, which led to a slight increase in $^{187}Os/^{188}Os$ in most samples, and to a substantial increase in samples TA54C1-3 and TA56. To verify these corrected ratios, unspiked duplicates of the low-Os pyroxenite samples were run (Table 1).

Multiple runs of Johnson–Matthey Os standard solution were measured along with every batch of samples analyzed. Over the course of several months, measured $^{187}Os/^{188}Os$ of this standard at the FUB using faraday cups was 0.11381 ± 0.00007 (2σ, $n = 29$). Measurements with the SEM yielded $^{187}Os/^{188}Os$ of 0.1138 ± 0.0003 (2σ, $n = 5$). At UMD, the Johnson–Matthey standard yielded $^{187}Os/^{188}Os$ of 0.1138 ± 0.0002 for both the VG Sector-54 (faraday cup runs) and the NBS mass spectrometer (SEM runs). Total procedural blanks ($n = 6$) were 4.8 ± 2.0 pg for Os with an $^{187}Os/^{188}Os$ of 0.170 ± 0.040. Osmium blank

Table 1
Whole rock major, trace element and Os isotopic composition data for Totalp pyroxenites.

Sample	Lithology		Al_2O_3	MgO	CaO	Mg#	S	Os	Ir	Ru	Pt	Pd	Re	$^{187}Re/^{188}Os$	$^{187}Os/^{188}Os$	2 sd	$^{187}Os/^{188}Os$ 160 Ma	γ_{Os} 160 Ma	TMa
TA-11A1	spl-websterite	b	8.97	26.2	11.7	0.891	0.07		0.69	1.90	5.47	14.2	0.93						
duplicate		b							0.68	1.76	5.28	13.5	0.97						
TA-11A2	spl-websterite	a	9.18	29.1	9.09	0.890	0.09	1.62	1.44	3.95	8.47	21.6	0.570	1.70	0.1521	0.0001	0.1476	16.9	1148
duplicate		b						1.63	1.39	3.20	8.12	20.6	0.545	1.61	0.1518	0.0001	0.1475	16.9	1214
TA-11B	spl-websterite	b	8.69	28.4	9.87	0.888	0.04	2.06	1.82	4.36	8.19	22.3	1.07	2.15	0.1514	0.0001	0.1457	15.4	831
duplicate		b							1.83	4.32	8.32	22.7	0.93						
TA-13B	spl-websterite	a	7.01	27.2	9.91	0.890	n.d.	2.40	1.96	4.14	3.99		0.533	1.07	0.1618	0.0001	0.1589	25.9	3006
duplicate		b							1.97	4.98	4.19	9.67	0.540						
TA-13D	spl-websterite	a	7.04	30.8	6.81	0.894	n.d.	2.31	2.08	4.46	7.01		0.639	1.34	0.1643	0.0001	0.1607	27.4	2330
duplicate		b							2.13	4.64	6.55	6.72	0.639						
duplicate		b						2.50	2.16	4.68	6.59	6.58	0.711	1.38	0.1615	0.0001	0.1578	25.1	2070
TA-36A	Websterite	a	7.84	20.4	15.1	0.903	n.d.	4.64	0.68	1.84	2.67	3.10	0.357	0.370	0.1250	0.0001	0.1240	−1.7	5348
TA-54A	Websterite	b	8.81	35.2	5.32	0.874	0.26	6.47	4.62	10.8	53.5	173	9.13	6.79	0.1666	0.0001	0.1485	17.7	372
TA-54B	Clinopyroxenite	b	12.3	22.6	14.0	0.875	n.d.	0.98	0.689	1.77	9.91	35.0	3.07	15.2	0.2156	0.0001	0.1751	39	360
TA-54C1	Clinopyroxenite	b	12.8	22.0	14.0	0.877	0.02	0.105	0.078	0.21	1.36	3.60	0.508	24.6	0.647	0.011	0.581	360	1281
duplicate		b													0.509	0.018			
TA-54C2	Clinopyroxenite	b	11.9	20.4	15.5	0.875	0.02	0.184	0.137	0.41	2.25	4.82	2.01	54.3	0.385	0.006	0.241	91	288
TA-54C3	Clinopyroxenite	b	13.1	18.9	15.8	0.860	0.05	0.671	0.509	1.40	5.87	17.0	7.92	53.2	0.294	0.004	0.152	20.3	190
duplicate		b													0.2953	0.0001			
TA-54D	Clinopyroxenite	b	12.9	17.8	17.3	0.850	0.09	0.295	0.224	0.607	3.10	5.96	1.01	16.8	0.389	0.002	0.344	172	954
dupicate		b													0.375	0.002			
TA-55C	spl-websterite	b	7.78	27.5	6.75	0.883	0.05	3.44	2.77	7.09	9.09	17.2	1.33	1.89	0.1348	0.0001	0.1298	2.8	313
TA-55D1	spl-gt-clinopyroxenite	b	12.7	21.5	12.6	0.867	0.05	0.519	0.406	0.935	3.81	12.2	1.96	18.9	0.279	0.002	0.228	81	493
TA-56	gt-clinopyroxenite	b	13.6	16.2	17.6	0.850	n.d.	0.108	0.062	0.216	1.33	4.01	1.31	77.4	2.472	0.005	2.265	1700	1807
duplicate		b													2.205	0.008			
TA-61	gt-clinopyroxenite	a	11.0	15.4	18.6	0.831	0.04	0.400	0.163	0.507	3.63		3.20	42.8	0.869	0.0010	0.754	498	1045
duplicate		b						0.240	0.156	0.468	3.82	11.4	2.69	62.7	0.884	0.003	0.725	475	727

n.d.: not determined.
Major element and S concentrations are given in wt%, HSE concentrations in ppb.
(a) Measured at UMD, (b) measured at FUB.

contributions to samples were <2% for Os-poor samples TA54C1 and TA56 and <1% for all other samples.

Repeated determinations of $^{187}Os/^{188}Os$ in Os-rich websterites agreed within < 2%. However, for Os-poor clinopyroxenites $^{187}Os/^{188}Os$ deviated by up to 23% for TA54C1, essentially due to large spike corrections.

For PGE and Re isotope dilution analyses, one third of the remaining acid phase fraction was carefully reduced in volume in Teflon beakers, converted to chloride by first using 8 ml 6 M HCl and then 8 ml 0.2 M HCl, and dried down. The samples were then taken up in 10 ml 0.2 M HCl and loaded onto ion exchange columns that contained 10 ml Eichrom AG50X-8 (100–200 mesh) cation exchange resin. While the PGE and Re passed the resin without interaction, most other elements were retained on the column (Meisel et al., 2003). The collected fraction was dried down on a hotplate at ~120 °C, taken up in 0.28 M HNO_3 and measured on an Element 2 (UMD) or Element XR (FUB) sector field ICP-MS instrument in low-resolution mode, using an Aridus membrane desolvation system. At FUB, Re was analyzed using a cyclonic glass spray chamber.

An analysis typically comprised 400 scans of masses 98, 99, 101, 102, 103, 104, 105, 106, 108, 110, 111, 185, 187, 189, 191, 193, 194, 195, 196, 197, 198 and 199. Isobaric interferences caused by Cd, Os and Hg on Pd, Re and Pt were insignificant in all cases. A mixed Re–Ir–Ru–Pt–Pd in house standard solution with roughly chondritic abundance ratios and ~1 ng/g Ir was analyzed multiple times during each analytical session and monitored over the course of several months. Isotopic ratios of samples were corrected for mass discrimination by the comparison of measured isotope ratios from the in-house standard solution with recommended values.

Washout time between samples was set between 3 and 5 min. On-peak zeroes for 0.28 M HNO_3 were taken after every 4–5 samples to monitor potential memory effects and were insignificant in all cases. Total chemistry blanks run in the course of this study ($n = 7$) were 7–12 pg for Re, 2.8–6.9 pg for Os, 0.3–7 pg for Ir, 2–20 pg for Ru, 2–440 pg for Pt and 42–420 pg for Pd. Blanks for Pt and Pd were substantially affected by the batch of Carius tubes used. With the exception of Os and Ir in samples TA54C1, TA54D2, TA54D and TA56, blank corrections were negligible or minor (<1%). Due to the high Pt and Pd contents of the samples, even the highest Pt and Pd blanks contributed less than 2%. Duplicates agreed within 2% for Os, 5% for Ir, 5% for Ru, 3% for Pt and 5% for Pd concentrations, but were worse for Os and Ru in TA61 and for Pd in TA13B. Rhenium reproducibility was strongly variable in duplicates, with values between 2% (TA11A2; TA13B) and 30% (TA61), see Table 1.

3.2. Electron microprobe

Microprobe analyses of sulfide grains in thick sections for S, Fe, Ni, Co and Cu abundances were conducted using the JEOL 8900 Superprobe at the University of Maryland with an acceleration voltage of 15 kV and probe current of 50 nA. Multiple spots were analyzed in each grain from both cores and rims to ensure internal homogeneity of sulfides for the subsequent LA-ICP-MS. Beam diameter was 1 μm. Chalcopyrite was used as calibration standard for Cu, pyrite for Fe and S, and Co and Ni were calibrated using Co and Ni metals. Raw intensities were corrected using ZAF. All elements were analyzed for 20 s on peak and 10 s on background, with the exception of Ni and Co, which were analyzed for 30 s on peak and 15 s on background.

3.3. Laser ablation-ICP-MS

Laser ablation data on the same sulfide grains used for microprobe analysis were obtained using a 213 nm laser ablation (LA) system coupled with an Element2 ICP-MS at the University of Maryland using He as a carrier gas.

Table 2
Sulfide major element compositions in websterites TA11A2 and TA54A.

Sample	Grain #	Mineral	# Analyses	S		Ni		Fe		Co		Cu	
				at%	2 sd	at%	2 sd	at%	2 sd	at%	2 sd	at%	2 sd
TA11A2	1	Pentlandite	5	56.2	0.6	21.2	0.4	21.8	0.5	0.76	0.05	0.08	0.07
	2	Pentlandite	3	55.3	0.6	20.7	0.1	22.5	0.5	1.34	0.09	0.10	0.06
	3	Pentlandite	5	54.8	3.2	19.4	1.6	25.3	4.8	0.44	0.05	0.11	0.10
	4	Pentlandite	4	56.0	0.5	21.7	0.3	21.8	0.2	0.47	0.06	0.07	0.05
	5	Pentlandite	2	55.7		22.2		21.1		0.95		0.08	
	6	Pentlandite	2	51.5		17.2		30.4		0.70		0.16	
	7	Pentlandite	8	56.5	1.2	20.2	1.2	22.6	1.2	0.56	0.31	0.10	0.05
TA54A	1	Godlevskite	4	43.5	2.7	53.3	2.9	1.5	3.5	0.13	0.21	1.6	5.1
	nc 2/4	Native copper	4	0.03	0.03	4.3	1.7	0.42	0.71	0.06	0.08	95.2	2.1
	3	Godlevskite	5	44.9	1.5	53.8	1.6	0.29	0.21	0.12	0.06	0.87	1.10
	4	Godlevskite	3	45.2	0.0	54.4	0.1	0.10	0.05	0.15	0.03	0.12	0.05
	5	Godlevskite	2	44.5		54.4		0.26		0.12		0.67	
	6	Godlevskite	8	46.5	2.3	52.8	2.8	0.07	0.08	0.14	0.64	0.47	1.00
	7	Godlevskite	10	45.0	1.5	54.0	2.2	0.44	0.64	0.26	1.03	0.28	0.49
	8	Godlevskite	1	45.3		53.3		0.60		0.10		0.68	

nc 2/4, native copper grain #2 (3 spots) and native copper associated with grain #4 (1 spot).

Table 3
Sulfide trace element compositions for websterites TA11A2 and TA54A.

Sample	Grain	Mineral	Spot size	Ru (ppm)	Pd (ppm)	Re (ppm)	Os (ppm)	Ir (ppm)	Pt (ppm)	Os/Ir	Pd/Ir	Ru/Ir	Re/Os	Re/Ir
TA11A2	1	Pn	40	0.81	2.77	0.35	0.10	0.06	<0.04	1.87	49.6	14.5	3.34	6.25
TA11A2	2	Pn	25	2.53	4.94	0.14	0.20	0.27	<0.12	0.77	18.5	9.49	0.67	0.52
TA11A2	2	Pn	25	0.84	4.61	0.14	0.15	0.11	<0.21	1.31	41.7	7.62	0.97	1.27
TA11A2	3	Pn	40	2.34	6.94	0.14	0.70	1.07	<0.07	0.65	6.5	2.18	0.20	0.13
TA11A2	3	Pn	40	3.27	7.80	0.09	1.03	1.19	<0.08	0.87	6.6	2.76	0.08	0.07
TA11A2	3	Pn	40	3.23	8.56	0.07	1.30	1.06	<0.04	1.22	8.1	3.04	0.06	0.07
TA11A2	3	Pn	30	1.72	7.88	0.09	0.84	0.83	<0.08	1.02	9.5	2.08	0.10	0.10
TA11A2	4	Pn	25	1.79	7.97	0.11	0.90	0.91	<0.16	0.99	8.7	1.96	0.12	0.12
TA11A2	5	Pn	30	4.90	5.48	0.20	2.33	1.44	<0.11	1.62	3.80	3.40	0.08	0.14
TA11A2	5	Pn	30	3.09	<0.17	0.11	1.43	1.40	<0.07	1.03	–	2.21	0.08	0.08
TA54A	4	Gdl	25	–	4.66	2.23	1.62	1.48	<1.66	1.09	3.1	–	1.38	1.51
TA54A	6	Gdl	40	–	4.98	9.14	3.63	3.39	<0.78	1.07	1.5	–	2.52	2.69
TA54A	6	Gdl	40	–	0.91	2.30	0.75	0.56	<0.11	1.33	1.6	–	3.05	4.07
TA54A	6	Gdl	25	–	1.65	0.53	0.09	0.09	<0.11	1.04	18.7	–	5.81	6.04
TA54A	6	Gdl	25	–	<0.25	0.12	0.04	0.03	<0.01	1.40		–	2.92	4.07
TA54A	7	Gdl	25	–	37.3	0.04	0.04	0.03	<0.02	1.66	1376	–	0.98	1.62
TA54A	7	Gdl	25	–	0.66	0.02	0.02	0.02	<0.02	0.98	26.7	–	0.67	0.66
TA54A	2	Cu	6	<2.04	15.9	<0.26	<0.45	1.35	0.07	–	–	–	–	–
TA54A	2	Cu	12	0.30	23.1	<0.05	<0.06	0.18	<2.58	–	–	–	–	–
Coahuila		Iron meteorite		25.9	2.2	1.1	12.1	19.6	36.2	0.62	0.11	1.32	0.09	0.14
		2 sd%		11.4	20.0	16.3	12.7	13.1	12.0	5.3	16.2	8.2	9.6	9.5
Brenan standard		Synthetic sulfide		288	313	85	357	378	323	0.94	0.83	0.76	0.24	0.25
		2 sd%		3.1	3.3	3.0	3.3	3.2	3.1	1.2	3.7	2.5	4.8	5.3

Pn: pentlandite, Gdl: godlevskite; Cu: native copper.

The sample gas flow was merged with Ar before injection into the plasma. Baselines were measured for about 60 s before ablation. Laser intensity was set to 45% (~2 J/cm^2) with a frequency of 8 Hz. Depending on grain size, spot size ranged between 6 and 40 μm (see Table 3 for details). The following masses were measured: ^{57}Fe, ^{59}Co, ^{61}Ni, ^{65}Cu, ^{75}As, ^{101}Ru, ^{103}Rh, ^{105}Pd, ^{185}Re, ^{187}Os, ^{188}Os, ^{190}Os, ^{193}Ir, ^{195}Pt and ^{197}Au.

Corrections for argides were minor for most analyses. Signals on ^{105}Pd in native Cu grains likely reflect interference from ^{65}Cu^{40}Ar, and were discarded. Similarly, interference of ^{61}Ni^{40}Ar on ^{101}Ru in Ni-rich godlevskites in TA54A was too high to determine Ru concentrations.

For internal standardization, Fe concentrations obtained by electron microprobe were used. As an external standard, polished sections of the iron meteorite Coahuila and a synthetical NiS sulfide bead (Brenan internal reference at UMD) were run four times each with each thick section analyzed by LA. A maximum of twelve spots were analyzed in each thick section. Trace element abundances were calculated using LAMTRACE software. External precision of HSE concentrations (2 sd) as documented by the reproducibility of external standards was better than 4% for all elements for the Brenan Standard. Reproducibility for the Coahuila iron meteorite was between 11% for Ru and 20% for Pd (Table 3). As the concentrations in Coahuila are closer to the concentrations in the analyzed sulfides, the Coahuila analyses provide a better estimate for the analytical uncertainty of the sulfide measurements. Reproducibility of HSE ratios was better, between 5% for Os/Ir and 16% for Pd/Ir (Table 3).

4. RESULTS

4.1. Whole rock compositions

Volatile-free calculated major element and HSE abundances are listed in Table 1, with original major element data included in the Electronic annex. Major element, Os and Re abundances as well as Os isotopic compositions of samples TA11A2, TA13B, TA13D and TA61 have previously been reported by van Acken et al. (2008). In the subsequent discussion, volatile-free calculated major element data are used.

Major element concentrations for Totalp samples are within the range reported for websterites and clinopyroxenites from massifs and xenoliths worldwide (Bodinier et al., 1987; Piccardo et al., 1988; Pearson et al., 1993; Becker, 1996; Santos et al., 2002; Xu, 2002). HSE concentrations in Totalp clinopyroxenites are similar to previously published HSE data for pyroxenites from other localities (Beni Bousera, Kumar et al., 1996; Pearson and Nowell, 2004; Luguet et al., 2008; Lower Austria, Becker et al., 2004), with the exceptions of samples TA36A and TA54A. Pyroxenite TA54 is a composite pyroxenite comprised of a Mg rich and Ca poor websterite layer (TA54A), spinel clinopyroxenite and Ca rich garnet–spinel clinopyroxenite. Websterite TA54A has very high concentrations for all HSE, particularly of Pt, Pd and Re, while the spatially associated clinopyroxenite, samples TA54B through D, are comparatively poor in HSE (Table 1). HSE ratios, however, are similar throughout the TA54 sample suite, regardless of concentration, with Re and Pd strongly enriched relative to Os and Ir. The other unusual sample TA36A has a very high Os content coupled with normal concentrations of the other HSE (Table 1).

The HSE contents of both Totalp websterites and clinopyroxenites generally correlate positively with each other (Fig. 1), likely reflecting variable modal abundance of sulfides. Good correlations exist between Os, Ir and Ru ($R^2 > 0.98$, not shown), but correlations between Pt, Pd, Re and Ir are less clear. Totalp websterites and clinopyroxenites define two different trends in the Re–Ir diagram (Fig. 1a). Rhenium contents in Al-poor pyroxenites (websterites) correlate with Ir contents with a shallow positive slope, whereas Al-rich pyroxenites (clinopyroxenites) define a positive trend with a much steeper slope.

If websterites and clinopyroxenites are combined, broad negative covariations exist between Al_2O_3 and Os, Ir, and Ru. Platinum and Pd show no covariation with Al_2O_3 in

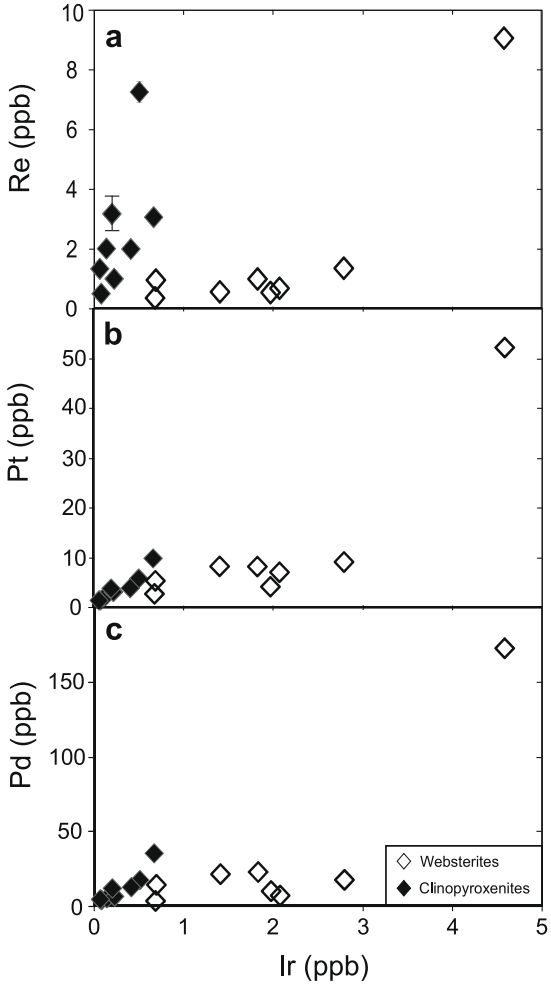

Fig. 1. Plots of (a) Re (ppb) vs. Ir (ppb), open symbols: Al-poor pyroxenites (websterites), filled symbols: Al-rich clinopyroxenites (see Table 1), (b) Pt (ppb) vs. Ir (ppb), (c) Pd (ppb) vs. Ir (ppb). Error bars are symbol size or smaller, except where shown.

the Totalp pyroxenites, while Re in high-Al_2O_3 clinopyroxenites tends to be higher than in low-Al_2O_3 websterites, with the exception of TA54A (Fig. 2). CI-normalized HSE/Ir ratios in the pyroxenites show broad positive correlations with Al_2O_3, with increasing scatter towards the Al-rich clinopyroxenites (Fig. 3), extending previously demonstrated correlations for lherzolites to higher Al_2O_3 values (Becker et al., 2006).

Totalp websterites show HSE patterns with moderate depletion of Os, Ir, Ru and Pt, compared to primitive mantle (PM) estimates, while Pd and Re are variably enriched. Some websterites have high Pd/Re, resulting sometimes in a positive Pd peak in the pattern (Fig. 4a), similar, but more pronounced, than the Pd excess found in some fertile lherzolites (e.g. Becker et al., 2006). Most HSE patterns in clinopyroxenites, except the anomalously Os-rich sample TA36A, show massive depletion in Os, Ir, Ru and Pt. While Pd and Re are enriched over the more compatible elements, these samples have low Pd/Re, reflecting a more "melt-like" or "basaltic" HSE pattern compared to the websterites (Fig. 4b; Bézos et al., 2005; Dale et al., 2008).

Measured $^{187}Os/^{188}Os$ range from 0.1250 to 2.4, comparable to pyroxenites from other suites (Kumar et al., 1996; Becker et al., 2004; Pearson and Nowell, 2004; Melcher and Meisel, 2004). Corrections for radiogenic ingrowth after formation are significant due to the high Re/Os in most samples. Initial $^{187}Os/^{188}Os$ calculated for a formation time of 160 Ma range from slightly subchondritic (0.1240) to extremely radiogenic (2.265), corresponding to γ_{Os} (160 Ma) values (γ_{Os} = % deviation from average chondritic composition, Walker et al., 1989) of −1.7 to +1700. A broad correlation exists between γ_{Os} (160 Ma) and $^{187}Re/^{188}Os$ (Fig. 5), with samples TA54C2 and TA54C3 offset to lower γ_{Os} (160 Ma) compared to the main trend. High-Al clinopyroxenites generally have higher γ_{Os} (160 Ma) than low Al websterites (Fig. 6) and associated peridotites (van Acken et al., 2008).

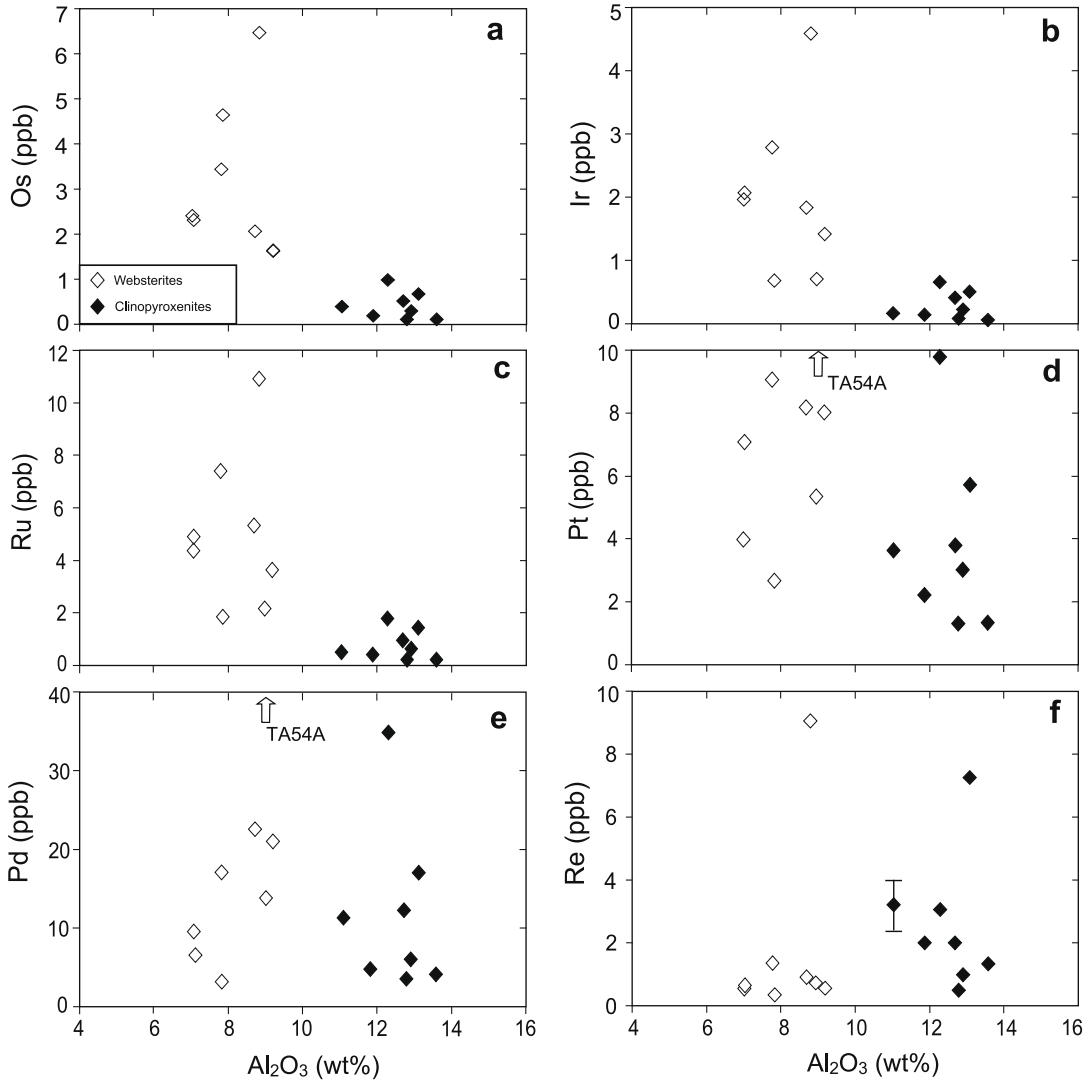

Fig. 2. (a–f) Plots of HSE abundances (ppb) vs. Al_2O_3 (wt%); open and filled symbols as in Fig. 1, TA54A not plotted in (d) and (e) for scale reasons. Error bars are symbol size or smaller, except where shown.

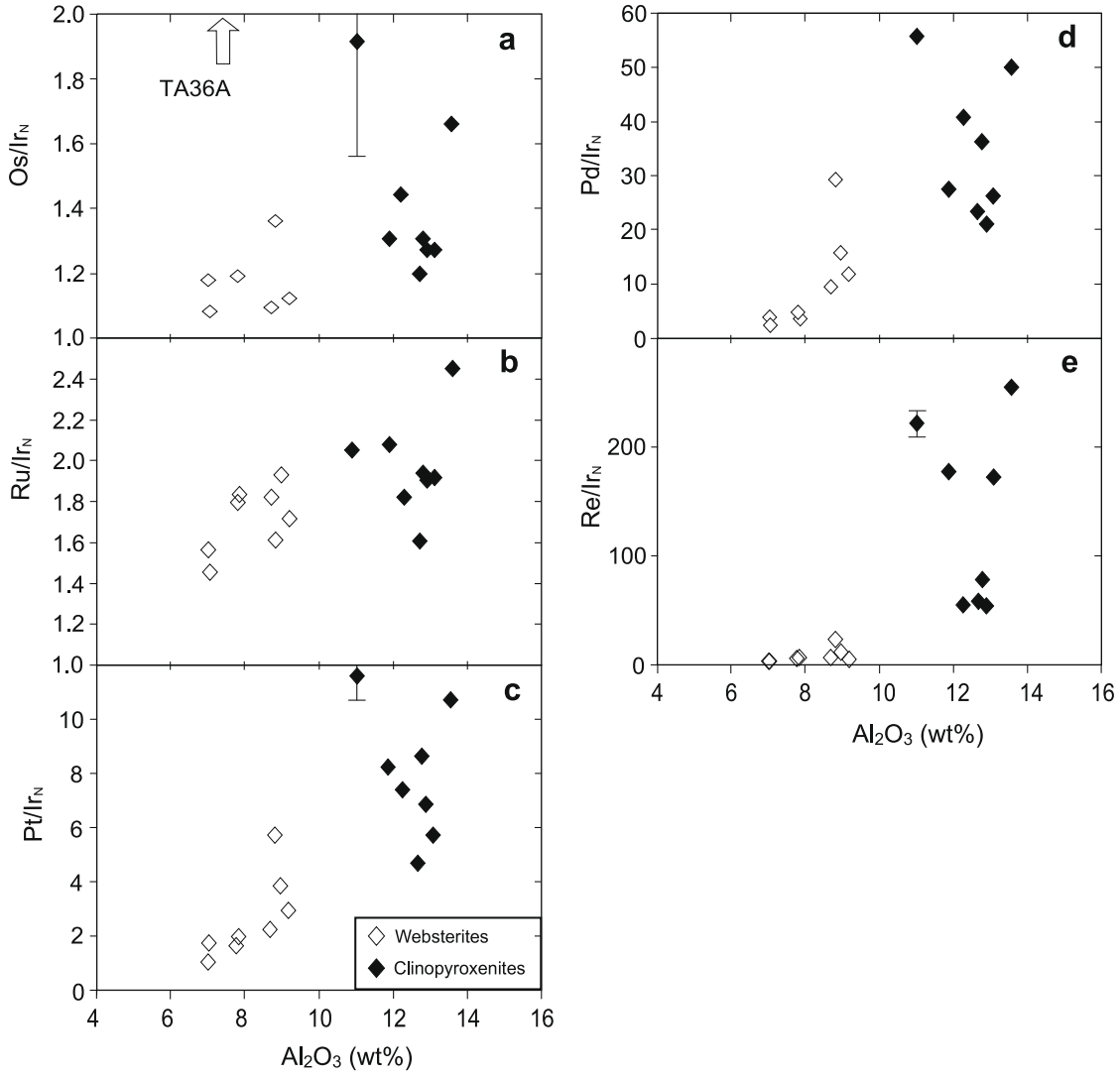

Fig. 3. (a–e): Plots of CI chondrite normalized HSE ratios vs. Al_2O_3 contents of the pyroxenites. The CI chondrite values in all figures are those of Horan et al. (2003); open and filled symbols as in Fig. 1. TA36A not plotted in a) for scale reasons. Error bars are symbol size or smaller, except where shown.

4.2. Sulfide compositions

Within the two analyzed websterite samples, major element compositions of sulfides from are remarkably homogeneous, both on thick section and grain scale (Table 2). Sulfide grains, found mostly on silicate grain boundaries, are anhedral and range from a few μm to 150 μm. Fe-bearing alteration phases such as magnetite and hematite occur along with sulfides in both thin sections.

Sulfides in TA11A2 are almost exclusively pentlandite with Ni and Fe in roughly the same proportion, while sulfides in TA54A predominantly consist of godlevskite (Ni_9S_8) intergrown with native copper and Ni-rich pentlandite in anhedral grains crosscut by serpentinite veins.

Sulfide grains in thick sections from TA11A2 and TA54A were analyzed for HSE by LA-ICP-MS (Table 3). Except for Pt, the HSE are about three orders of magnitude more abundant in sulfides than in whole rocks, as might be expected from their modal abundance. While major elements in sulfides are homogeneously distributed on the grain scale, this does not hold true for the HSE. Within section TA11A2, Re and Pd concentrations in sulfides show little variation, whereas concentrations of Os, Ir and Ru vary over about an order of magnitude. In TA54A, all HSE are heterogeneously distributed, with the range spanning over two orders of magnitude. While some sulfide grains show enrichment of all HSE determined, other grains show extreme enrichment of only Pd. HSE in sulfides show no systematic correlation with the major element composition of sulfides.

Two grains of native copper were sampled in TA54A. Because of the small grain sizes of native copper, smaller beam diameters had to be used and thus, lower signal intensities were achieved. Concentrations of Os, Re and Ru in native Cu are lower than the detection limit, while Ir is in a similar range compared to the pentlandites. High signals on Pd mass 105 likely reflect $^{65}Cu^{40}Ar$.

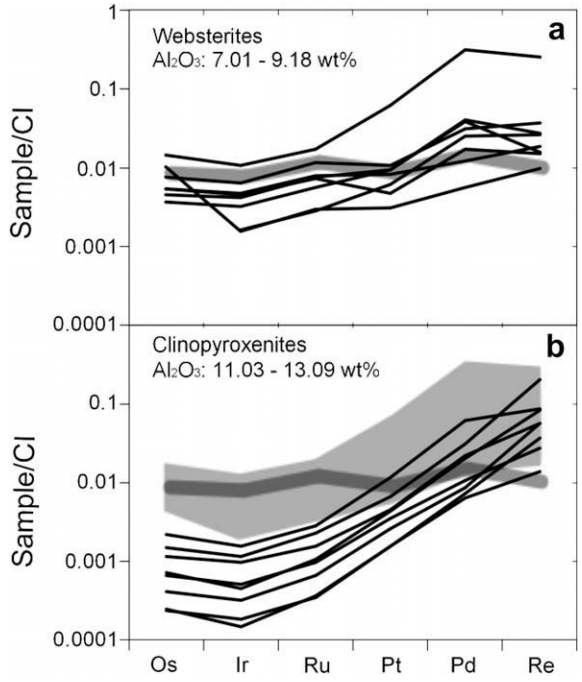

Fig. 4. Plots of (a) CI-normalized HSE patterns for Totalp websterites; grey solid line: primitive mantle (PM) model composition after Becker et al. (2006); (b) CI-normalized HSE patterns for Totalp clinopyroxenites, shaded area: websterites from Fig. 4a.

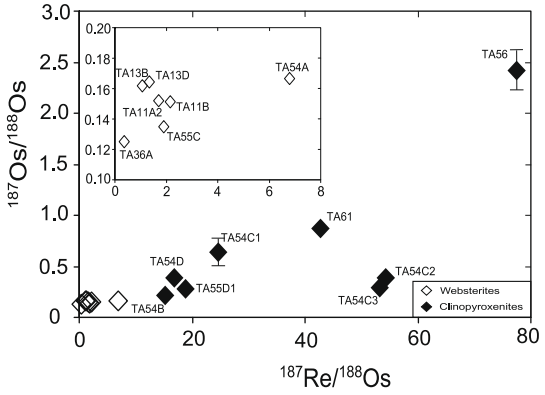

Fig. 5. Plot of $^{187}Os/^{188}Os$ vs. $^{187}Re/^{188}Os$; Regression of the pyroxenites (not shown), excluding two samples at the bottom right (TA54C1 and TA54C2), yields an apparent age of 1740 ± 370 Ma with initial $^{187}Os/^{188}Os$ of 0.01 ± 0.15, strongly indicating non-isochronous relationship of Totalp pyroxenites; open and filled symbols as in Fig. 1. Error bars are symbol size or smaller, except where shown.

None of the sulfides or native copper grains yielded detectable Pt signals. Calculated values are maximum values based on detection limits. Platinum has been shown to exsolve into micronuggets under subsolidus conditions (Luguet et al., 2001, 2003, 2007; Lorand et al., 2008; Dale et al., 2009). Subsequent BSE scans of the thick sections failed to detect any Pt-rich minerals in the section plane.

Os/Ir ratios in sulfides from both samples often lie within the chondritic range, with moderately subchondritic and

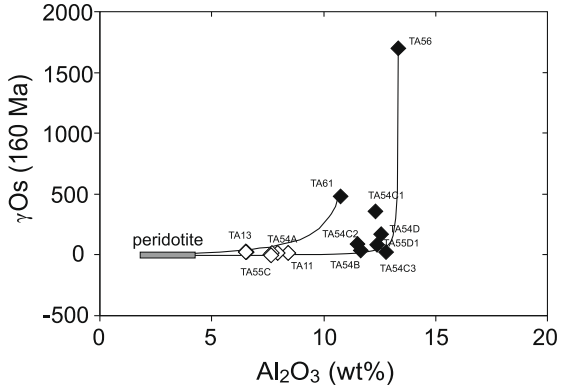

Fig. 6. Plot of γ_{Os} (160 Ma) vs. Al_2O_3, symbols as in Fig. 1; solid lines denote binary mixing between depleted peridotite with approximately chondritic γ_{Os} (160 Ma) and the most radiogenic pyroxenites from our dataset as approximations of melt composition (TA56, TA61), isotopic compositions for Totalp pyroxenites are similar to γ_{Os} reported in pyroxenites from other locations (Beni Bousera, Kumar et al. (1996) and Luguet et al. (2008); lower Austria, Becker et al. (2004); Speik Complex, Eastern Alps, Melcher and Meisel (2004)); open and filled symbols as in Fig. 1. Error bars are smaller than symbol size.

suprachondritic values occurring as well. Ru/Ir was determined only in TA11A2, and ranges from chondritic to suprachondritic values. While some of the Ru data from TA54A were significantly affected by interferences from NiAr, high Ru/Ir in some TA11A2 sulfides is due to low Ir concentration in these grains. Most sulfides in these samples have lower Pd/Ir than the corresponding whole rock ratios of 13.6 and 33.3, thus balancing a few grains with extremely high Pd/Ir. Re/Ir in both samples scatter around the corresponding whole rock ratios (Table 3; Fig. 7).

The websterites are devoid of chalcopyrite, which has been observed to be a prominent sulfide and host of Pd in previous studies of mantle peridotites (Lorand, 1989; Alard et al., 2000; Luguet et al., 2001, 2003, 2007). This is unexpected in the context of the high Pd contents observed in Totalp pyroxenites, but may reflect different bulk compositions and subsolidus metamorphic reactions.

5. DISCUSSION

5.1. Modeling Totalp pyroxenite formation with HSE

Pyroxenites have been interpreted to represent residues of melting of eclogitic layers or to represent precipitates from melts related or unrelated to surrounding peridotites. Like many other pyroxenites and associated peridotites the Totalp samples display broadly linear major element covariations. These variations do not provide much information that might help in distinguishing the aforementioned formation models. Formation of the pyroxenites by in situ crystallization of partial melts of the host peridotite was suggested for some pyroxenites from the Balmuccia peridotite body (Sinigoi et al., 1983; Voshage et al., 1988). If this was the case for the Totalp pyroxenites, the peridotites and pyroxenites should have been in isotopic equilibrium at the

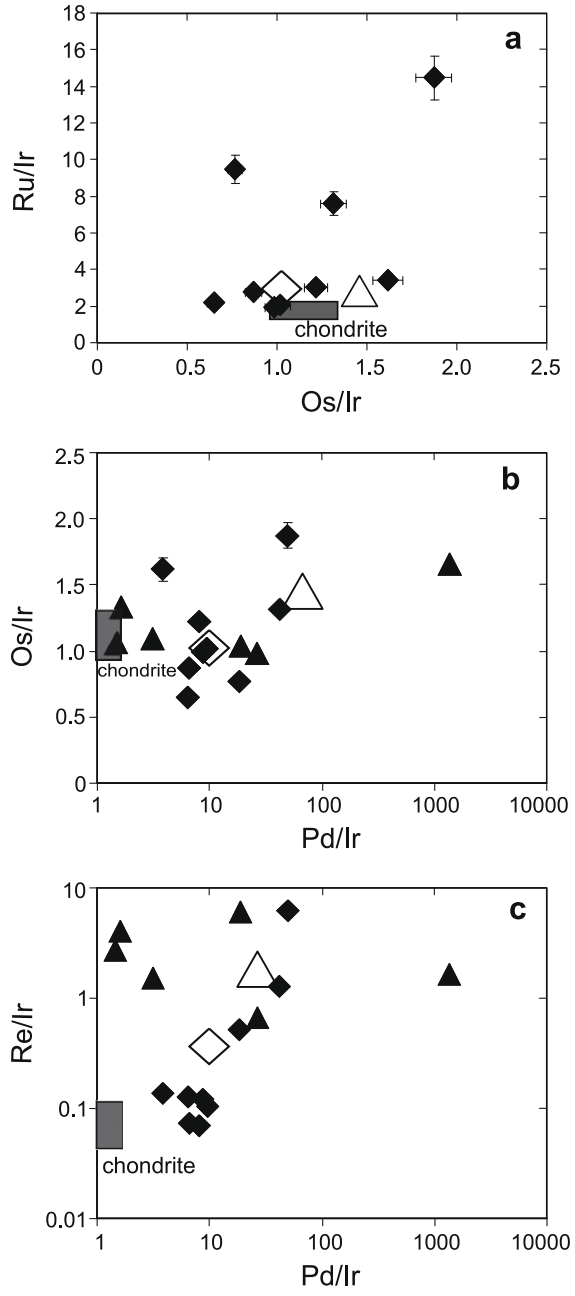

Fig. 7. (a-c): Plots of inter-element HSE ratios for sulfides from TA11A2 (diamonds) and TA54A (triangles), closed symbols: individual sulfide measurements, open symbols: corresponding bulk rock, gray shaded field: chondrite composition after Horan et al. (2003). Error bars are symbol size or smaller, except where shown.

time of pyroxenite formation, which may have been the Jurassic or late Paleozoic (Peters and Stettler, 1987; Müntener et al., 2004). Large differences in initial γ_{Os} between Totalp peridotites and pyroxenites (Table 1; Fig. 6; van Acken et al., 2008), however, preclude a simple melt–residue relationship at any time during the Phanerozoic. A main argument for a Jurassic or at most late Paleozoic age of the igneous processes in the Totalp body is the presence of asthenosphere-derived igneous rocks (gabbros, pillow basalts, alkali basalts) that formed during the prolonged Carboniferous to Cretaceous extensional period in the Alpine Tethys realm (Manatschal and Bernoulli, 1998, and references therein). These magmatic processes should have left their mark in the mantle rocks of this area (e.g. Schaltegger et al., 2002; Müntener et al., 2004).

The Totalp pyroxenites are characterized by strong fractionation of HSE relative to both chondrites and primitive mantle estimates (Fig. 4). Compared to PM, the pyroxenites are enriched in Re and Pd, and mostly depleted in Os, Ir and Ru. Most samples are also characterized by suprachondritic initial $^{187}Os/^{188}Os$. The two samples analyzed for in situ HSE distribution are characterized by a heterogeneous HSE distribution on the thin section scale, possibly indicating the presence of multiple sulfide generations or small scale heterogeneities due to a complex subsolidus history of the sulfides.

In light of the radiogenic Os isotope and HSE abundance characteristics outlined above, we more closely consider the other two models for Totalp pyroxenite formation: (a) formation as residues of partial melting of eclogitic oceanic crust (Dick and Sinton, 1979; Polvé and Allègre, 1980; Allègre and Turcotte, 1986; Blichert-Toft et al., 1999) and (b) formation as products of melt–rock interaction, either as cumulate precipitates or melt–rock reaction products, between depleted mantle peridotite and mafic melt (e.g. Obata, 1980; Sinigoi et al., 1983; Suen and Frey, 1987; Takazawa et al., 1999).

Derivation of the pyroxenites from recycled oceanic crust with high Re/Os (Roy-Barman and Allègre, 1994; Schiano et al., 1997; Escrig et al., 2005; Gannoun et al., 2007), either as residues of partial melting or as partial melts, is consistent with the radiogenic initial γ_{Os} in most Totalp pyroxenites. Residues of partial melting should be characterized by enrichment in compatible HSE, such as Os, Ir and Ru over their precursor material, and accompanied by depletions in incompatible HSE, such as Pd or Re. In contrast, partial melts would be expected to be enriched in Pd and Re. If the pyroxenites are products of interactions between mafic melts and peridotite, the HSE signature of the resulting rocks to some degree should reflect the mixed HSE characteristics of the mafic melt and peridotite.

In order to distinguish between the two models of pyroxenite formation, we model HSE abundances in both a melt and a residue resulting from the partial melting of a basic rock with an original HSE composition similar to that of subducted MORB. A representative HSE composition of subducted oceanic crust was calculated from datasets of HSE abundances in MORB (Schiano et al., 1997; Rehkämper et al., 1999a; Bézos et al., 2005; Escrig et al., 2005; Gannoun et al., 2007; Dale et al., 2008). HSE abundances reported for lower oceanic crust, represented by gabbros or gabbroic eclogites, with higher Os abundances and similar Re abundances compared to MORB, were also taken into account (Blusztajn et al., 2000; Dale et al., 2007). As HSE concentrations in MORB vary by as much as two orders of magnitude, the choice of starting composition for the model strongly influences the model outcome (Fig. 8). For the modeling, we chose a representative MORB composition, which is listed in Table 4. Both batch and

fractional melting of MORB were modeled using equations derived by Shaw (1970). We will limit discussion to the fractional melting model, as batch and fractional melting produce similar results for these elements.

As noted above, the HSE are strongly chalcophile under upper mantle conditions (Garuti et al., 1984; Peach et al., 1990, 1994; Barnes, 1993; Bezmen et al., 1994; Fleet et al., 1999; Sattari et al., 2002; Andrews and Brenan, 2002; Pruseth and Palme, 2004; Brenan, 2008). Consequently, in the following models solid sulfide–liquid sulfide partitioning is assumed to control HSE distribution (e.g. Bockrath et al., 2004), and, with the exception of Re, silicate–sulfide partitioning of HSE is assumed to be negligible. While Os, Ir, Ru and Re are compatible in mss during partial melting, with $D^{\text{mss/sulfide melt}}$ of about 2–10, Pt and Pd are incompatible with $D^{\text{mss/sulfide melt}}$ of ~0.1–0.25 (Fleet et al., 1993; Li et al., 1996; Brenan, 2002, 2008; Bockrath et al., 2004; Mungall et al., 2005; Ballhaus et al., 2006). Subsequent separation of sulfide melt from residual mss can result in fractionated patterns in both melt and residual sulfide (Bockrath et al., 2004; Ballhaus et al., 2006).

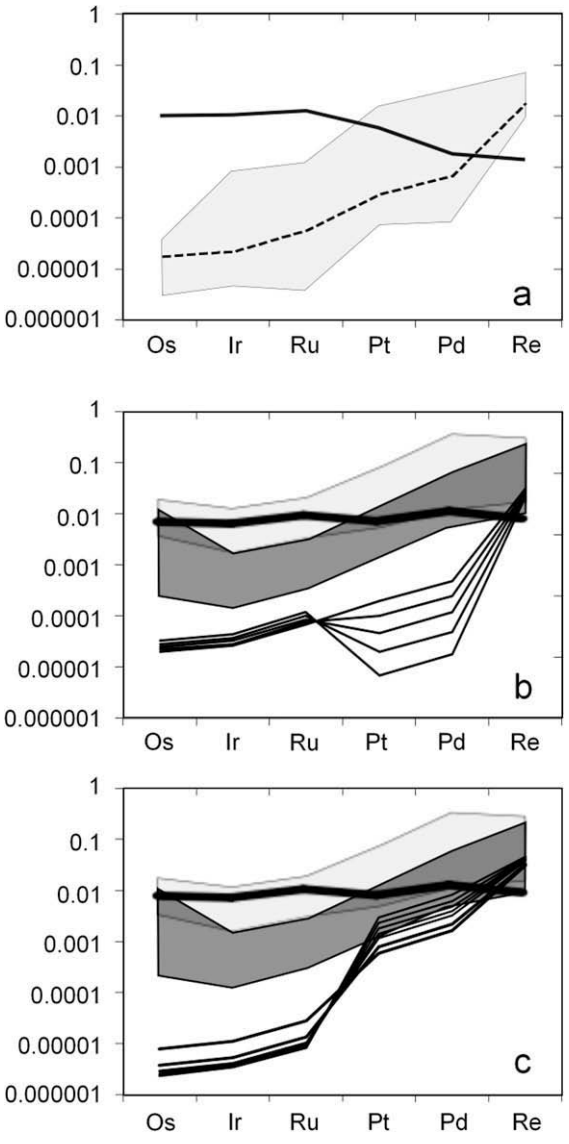

Fig. 8. (a) CI-normalized HSE patterns for typical mid-ocean ridge (dashed line), depleted peridotite (solid line, e.g. Pearson et al., 2004; Luguet et al., 2007); shaded area: range of MORB composition reported worldwide (Schiano et al., 1997; Rehkämper et al., 1999a; Bézos et al., 2005; Escrig et al., 2005; Dale et al., 2007; Gannoun et al., 2007). Depleted peridotite HSE composition: 4.5 ppb Os, 4.5 ppb Ir, 8 ppb Ru, 4 ppb Pt, 1 ppb Pd and 0.05 ppb Re. MORB HSE composition: 0.008 ppb Os; 0.01 ppb Ir, 0.04 ppb Ru, 0.3 ppb Pt, 0.5 ppb Pd, 1 ppb Re; (b) composition of residues for 1 to 50% fractional melting of subducted MORB; (c) corresponding partial melts. Equations for melting were taken from Shaw (1970). Thick solid line in (b) and (c): Primitive upper mantle composition (Becker et al., 2006); Light shaded field in (b) and (c): Totalp websterites; dark shaded field in (b) and (c): Totalp clinopyroxenites.

Rhenium, as the most lithophile element among the HSE may be incorporated in silicate minerals (Righter and Hauri, 1998; Righter et al., 2004; Mallmann and O'Neill, 2007). Recent studies report a strong dependence of Re partitioning behavior on oxygen and sulfur fugacities, suggesting that Re behavior is controlled by both the redox state of Re and sulfur speciation in the mantle (Amossé et al., 2000; Brenan, 2002, 2008; Fonseca et al., 2007; Mallmann and O'Neill, 2007). Experimentally determined sulfide–silicate partition coefficients for Re vary over three orders of magnitude, depending on experimental conditions (Fleet et al., 1999; Sattari et al., 2002; Fonseca et al., 2007; Brenan, 2008). For typical lower oceanic lithosphere redox conditions of log fO_2 values of -1 relative to the QFM buffer (e.g. Lee et al., 2003), the sulfide-silicate melt partition coefficient D_{Re} may be as low as 300, compared to $D_{Re} > 1000$ at more reducing conditions, thus, resulting in a significant proportion of Re hosted in garnet and/or clinopyroxene (Righter and Hauri, 1998; Sattari et al., 2002; Fonseca et al., 2007; Mallmann and O'Neill, 2007). During melting of an eclogitic source, bulk partitioning of Re will, thus, be controlled by complex sulfide solid–sulfide melt–garnet–clinopyroxene–silicate melt partitioning, the solubility of sulfide in silicate melt, and sulfide exhaustion.

Sulfide contents of eclogites vary over a wide range, with a maximum around 900 ppm (Greau et al., 2008), which has been adopted as the model starting parameter. Rhenium concentration in sulfides varies widely between 30 and 4200 ppb (Richardson et al., 2001; Aulbach et al., 2009). A sulfide Re concentration of 400 ppb corresponds to 1 ppb whole rock concentration, in broad accordance with observed values in basalts (Roy-Barman and Allègre, 1994; Schiano et al., 1997; Escrig et al., 2005; Dale et al., 2008). A value of 600 for $D_{Re}^{\text{sulfide/silicate}}$ was chosen for Re distribution in the starting eclogite composition, in accordance with experimental studies (Fonseca et al., 2007; Brenan, 2008). For an eclogitic source rock with 80% clinopyroxene and 20% garnet (Pertermann and Hirschmann, 2003), this results in only 32% of Re residing in sulfide, compared to 55% in clinopyroxene and 13% in garnet. Additional minor phases studied during experimental melting of eclogite, such as quartz/coesite and rutile (Pertermann and Hirschmann, 2003), have not been considered for the melting model, as they are not significant hosts for HSE.

Table 4
Model parameters.

	Os	Ir	Ru	Pt	Pd	Re	Sulfide (ppm)
MORB/eclogite	0.008	0.01	0.04	0.3	0.5	1	900
Depleted peridotite	4.5	4.5	8	4	1	0.05	200
$D_{cpx/melt}$	–	–	–	–	–	0.5	
$D_{gt/melt}$	–	–	–	–	–	0.5	
$D_{sulfide\ solid/sulfide\ melt}$	8	8	8	0.15	0.15	3	
$D_{sulfide/silicate}$	30,000	40,000	20,000	15,000	30,000	600	

HSE concentrations are in ppb.

In order for sulfide melt–mss fractionation to be applicable, sulfide melt and sulfide solid must coexist throughout the melting process. Comparisons of S concentrations in eclogites and S solubility in silicate melt under pressures of 2 GPa or higher show that sulfide phases should be present throughout the melting process considered here (Haughton et al., 1974; Wendlandt, 1982; Wallace and Carmichael, 1992; Mavrogenes and O'Neill, 1999; Holzheid and Grove, 2002; O'Neill and Mavrogenes, 2002; Liu et al., 2007), making the HSE fractionation model suggested by Bockrath et al. (2004) and Ballhaus et al. (2006) applicable.

Modeling is further complicated by uncertainty of the relative solidus and liquidus temperatures for silicate and sulfide components, respectively. Dry eclogite compositions have experimentally been shown to have solidus temperatures at 3 GPa of approximately 1300 °C, and liquidus temperatures of 1425–1500 °C, with increasing temperatures with higher pressure (Yasuda et al., 1994; Pertermann and Hirschmann, 2003). Addition of H_2O results in considerably lower solidus (as low as 800 °C) and liquidus (1100 °C) temperatures (e.g. Rapp and Watson, 1995).

Sulfide solidus and liquidus temperatures for Ni-poor sulfides at atmospheric pressure are around 850–1100 °C (Ballhaus et al., 2001). Both sulfide solidus and liquidus increase significantly with pressure, with Ni-rich sulfides at pressures up to 3 GPa having solidus temperatures of about 1300 °C, comparable to silicate compositions (Bockrath et al., 2004). Sulfides and silicates can thus be expected to display approximately the same degrees of melting at a given temperature and pressure. Sulfides in eclogites display a wide range of major element composition, with sulfide grains containing 4–25 at% Ni occurring in single eclogite samples (Aulbach et al., 2009). Nickel contents around 15% in sulfides are confirmed by Ni contents in clinopyroxene and garnet in eclogites (O'Reilly and Griffin, 1995) and $D_{Ni}^{sulfide/silicate}$ values around 300 for mafic assemblages (Rajamani and Naldrett, 1978). The application of experimentally determined partition coefficients is thus legitimate for our models, as the sulfide compositions observed in basalts and eclogites (Roy-Barman et al., 1998; Richardson et al., 2001; Aulbach et al., 2009; Dale et al., 2009) and those used for experiments overlap (Fleet et al., 1999; Mungall et al., 2005; Ballhaus et al., 2006).

Fractional melting of the silicate and sulfide portions of the eclogite source was modeled separately, and the resulting melts were combined. A detailed description of the modeling is given in the Electronic annex.

One to 50% melting of a MORB-type source produces residues depleted in all elements except for Re (Fig. 8b), as compared to primitive mantle. While Re concentrations in model residues are within the same range as those of Totalp websterites, modeled concentrations of all other HSE are significantly lower than in the websterites. Depletions in Os, Ir and Ru are inherited from the starting composition of the model, while depletions in Pt and Pd result from their incompatibility and preferred partitioning into sulfide melt. The modeled HSE signatures from residues of partial melting of recycled oceanic crust contrast with the Pt, Pd- and Re-enriched signatures observed in Totalp websterites and clinopyroxenites (Figs. 3 and 4). As our model results did not take into account possible loss of HSE during subduction, (e.g. Becker, 2000; Dale et al., 2008), HSE concentrations might be even lower. An origin as residues from partial melting of subducted oceanic crust, thus, appears unlikely based on the HSE signatures of the pyroxenites.

A number of studies suggest a pyroxenite origin by cumulate precipitation (Irving, 1980; Bodinier et al., 1987, 1990; Takahashi, 1992; Pearson et al., 1993; Vaselli et al., 1995; Becker, 1996; Kumar et al., 1996; Garrido and Bodinier, 1999) or melt–rock reaction (Yaxley and Green, 1998; Garrido and Bodinier, 1999). While simple mixing of depleted peridotite and basaltic melt fails to reproduce the high concentrations of Pt, Pd and Re observed in some Totalp pyroxenites, cumulate precipitation of pyroxenes and sulfides in zones of increased melt flow may be a possible mechanism. Rehkämper et al. (1999b) suggested precipitation of sulfides from a basaltic melt during multiple episodes of melt–rock interaction in an open system. Based on Nd isotope systematics of refertilized Totalp peridotites, Müntener et al. (2004) suggested a MORB-like composition for the infiltrating melts.

For modeling accumulation and melt–rock interaction, a representative harzburgite composition was chosen as the depleted endmember, as even the most depleted Totalp lherzolites may have been affected by refertilization. The HSE patterns for the harzburgitic endmember used in the modeling are characterized by pronounced depletion of Pt, Pd and Re relative to Os, Ir and Ru (Table 4; Pearson et al., 2004; Luguet et al., 2007).

Using the melting model outlined above, model HSE patterns for partial melts of eclogitic recycled crust are characterized by further enhancement of the Pt, Pd and Re enrichments inherited from their basaltic precursors. With increasing degrees of partial melting, HSE patterns in the melt trend towards the pattern of the basalt

(Fig. 8). Given the lower liquidus of eclogites and sulfides compared to mantle peridotite (Yasuda et al., 1994; Yaxley and Green, 1998; Pertermann and Hirschmann, 2003; Kogiso et al., 2003, 2004), large degrees of melting seem to be more applicable, resulting in melts of broadly basaltic melt composition.

For modeling sulfide precipitation from basaltic melts, we have adopted the model and parameters by Rehkämper et al. (1999b). Multiple batches of basaltic melt were assumed to precipitate 50 ppm of sulfide in equilibrium from each batch of S-saturated melt. Representative sulfide–silicate partition coefficients for PGE were chosen from experimental literature data ($D_{HSE}^{sulfide/silicate\ melt}$: Os: 30,000; Ir: 40,000; Ru: 20,000; Pt: 15,000; Pd: 30,000) and $D_{Re}^{sulfide/silicate} = 600$; Bezmen et al., 1994; Peach et al., 1994; Fleet et al., 1999; Andrews and Brenan, 2002; Sattari et al., 2002; Pruseth and Palme, 2004; Fonseca et al., 2007; Brenan, 2008). Published $D_{HSE}^{sulfide/silicate\ melt}$) values show variation of at least half an order of magnitude. Some authors suggested $D_{HSE}^{sulfide/silicate\ melt}$ several orders of magnitude higher based on HSE solubility in sulfide liquids and metal/silicate partitioning (Ru, Andrews and Brenan, 2002; Pt, Pruseth and Palme, 2004), experimental partitioning (Ir, Bezmen et al., 1994) or observation in natural samples (Os, Hart and Ravizza, 1996). As even the lower D values of around 10^4 result in effective imprint of the melt signature on precipitating sulfide, use of the highest values up to 10^8 has only minuscule effects on the model outcome.

Partitioning of HSE during melting of either peridotitic or mafic mantle sources may be controlled by mss–sulfide melt equilibrium under S saturated conditions (Bockrath et al., 2004). Due to increasing solubility of sulfur in silicate melt with decreasing pressure, melts may become S-undersaturated upon ascent (Mavrogenes and O'Neill, 1999; Holzheid and Grove, 2002; O'Neill and Mavrogenes, 2002). In a closed system, precipitation of sulfide from S-undersaturated melts needs to be preceded by precipitation of silicate phases to drive the melt toward S-saturation. Sulfide precipitates from a sulfur saturated melt should carry the HSE signature of the melt, as HSE abundances in sulfides would no longer be controlled by $D_{HSE}^{mss/sulfide\ melt}$, but by $D_{HSE}^{sulfide/silicate\ melt}$.

Consequently, mss–sulfide melt equilibrium was assumed to have no influence on HSE behavior upon crystallization of sulfide. Segregation of sulfides that are not in equilibrium with surrounding silicate melt, either because of mechanical entrainment or because they are enclosed in silicates or oxides during their transport in the melt, would make it difficult to assess HSE compositions of parental melts (Campbell and Naldrett, 1979). Bulk rock HSE patterns of pyroxenites from Totalp display systematic behavior (e.g. clinopyroxenite samples TA 54 B to D with different major element compositions and variable γ_{Os}) and thus, do not support disequilibrium models that argue for arbitrary entrainment of sulfides.

Mixture of model cumulates from multiple melt batches with small amounts of residual depleted peridotite containing 200 ppm sulfide (Pearson et al., 2004; Luguet et al., 2007)) match the observed Totalp pyroxenite HSE patterns fairly well, although not perfectly. Websterites can be modeled as mixtures of 5–30% of depleted peridotites, with cumulates from 5–20 batches of melt derived from 20% partial melting of an eclogite source (Fig. 9a). Clinopyroxenites show an even stronger melt affinity and generally contain less than 5% contribution from peridotite host rock and 5–20 batches of basaltic melts formed by high degrees of partial melting (~80%) of an eclogite source (Fig. 9b). Formation of pyroxenites as cumulates in zones of high melt/rock ratio is thus most consistent with observed HSE signatures. Resulting sulfide abundances are between 400 and 1500 ppm, in good agreement with observations in Totalp websterites and pyroxenites, the sole exception being the anomalous sample TA54A (Table 1).

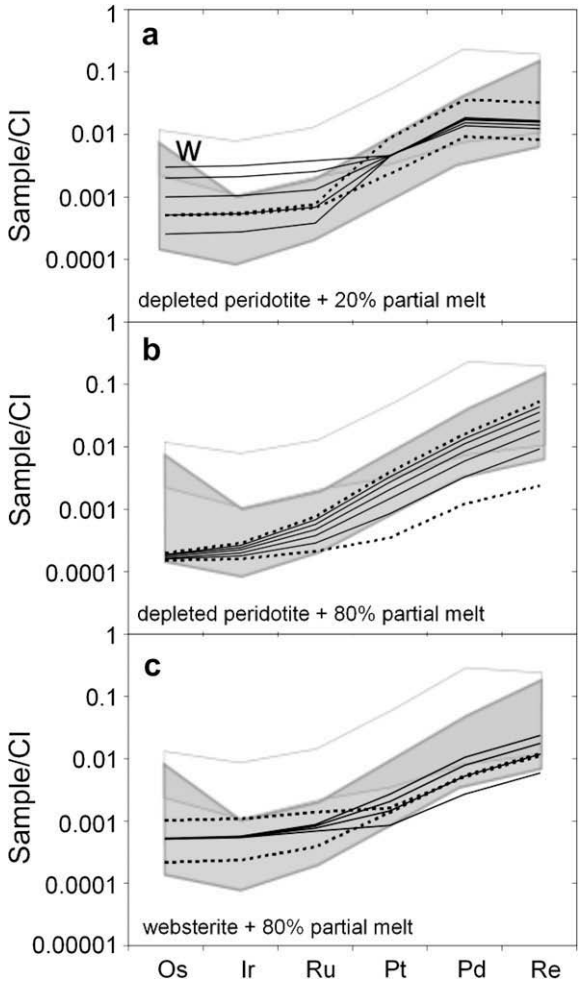

Fig. 9. Model results for (a) mixing of 20% partial melt derived from eclogite with depleted peridotite; solid lines (bottom to top): mixing of cumulates from 10 batches of melt with 2.5%, 5%, 10%, 20% and 30% of depleted peridotite; dashed lines: mixing of cumulates from five batches (lower dashed line) and 20 batches (upper dashed line) with 5% depleted peridotite. (b) mixing of 80% partial melt derived from eclogite with depleted peridotite; solid line (botton to top): mixing of cumulates from 5, 10, 15 and 20 batches of melt with 5% of depleted peridotite, dashed lines (bottom to top): mixing of cumulates from 20 batches of melt with 1%, 2% and 10% of depleted peridotites. (c) mixing of 80% partial melt derived from eclogite with websterite W (as indicated in (a)), lines and mixing proportions as in (b).

Several features observed in Totalp websterites and clinopyroxenites, however, could not be satisfactorily reproduced with this model. Neither the significant range of compatible HSE concentrations in clinopyroxenites nor the enrichment of Os over Ir, as observed in nearly all samples, can be replicated with the model. As these elements are largely controlled by the assumed concentration in the peridotitic endmember, the variation may reflect the degree of heterogeneity in the peridotite wall rock. In order to produce Os/Ir such as observed in Totalp pyroxenites by the processes discussed above, either Os/Ir in the peridotite wall rock is required to be between 1.2 and 1.7, or $D_{os}^{sulfide/silicate}$ needs to be as high as 150,000, compared to the value of ~30,000 derived from experiments. Similarly, high Ru/Ir values in Totalp pyroxenite require either Ru/Ir of 3 or higher in the wall rock peridotite or $D_{Ru}^{sulfide/silicate}$ of about 150,000–200,000, an order of magnitude higher than values commonly reported and than corresponding $D_{Ir}^{sulfide/silicate}$, but closer to the high D values determined by Andrews and Brenan (2002). Neither of these explanations seems fully satisfactory, as both depleted peridotites with such high Os/Ir and Ru/Ir are rarely observed, and $D_{HSE}^{sulfide/silicate}$ values for Os and Ru on the one hand and Ir on the other hand have not been shown to differ by an order of magnitude.

In situ HSE data for sulfides from two websterites show a larger variability of Pd/Ir and Re/Os than of Os/Ir and Ru/Ir than whole rock samples. Furthermore, the sulfides show a spectrum of compositions that range from "lherzolitic" in Os/Ir, Ru/Ir and Re/Ir, to suprachondritic for HSE ratios (Fig. 7). Compositional variability within each sulfide grain (Table 3) most likely reflects subsolidus partitioning processes, as described in previous studies (Luguet and Lorand, 1999; Luguet et al., 2001). The variation of Os/Ir, Re/Os and Pd/Ir from grain to grain (Table 3), however, is consistent with the presence of two sulfide endmember compositions on the thin section scale. Sulfides with "peridotitic" Os/Ir, Ru/Ir, and Re/Os and moderately suprachondritic Pd/Ir (most notable in websterite TA11A2), contrast with melt-derived sulfides in which most ratios are suprachondritic. Os/Ir, which in sulfides ranges from subchondritic to suprachondritic, displays chondritic to suprachondric values in whole rock compositions (Fig. 3). Because ratios of the HSE in whole rocks of the pyroxenites also indicate binary mixing of two distinct HSE components (Fig. 10), it is plausible that the whole rock variations are also controlled by two sulfide populations (Figs. 2, 3, 6 and 10). Websterites contain a larger fraction of HSE components derived from peridotite, whereas in clinopyroxenites, the inferred melt composition dominates the HSE budget. Curved correlations as evident in Fig. 10 d) indicate that in addition to mixing, chemical fractionation may have affected the distribution of some HSE (e.g. Pt vs. Re, Pd vs. Os); either during formation of the clinopyroxenites and/or during the evolution of their parental melts.

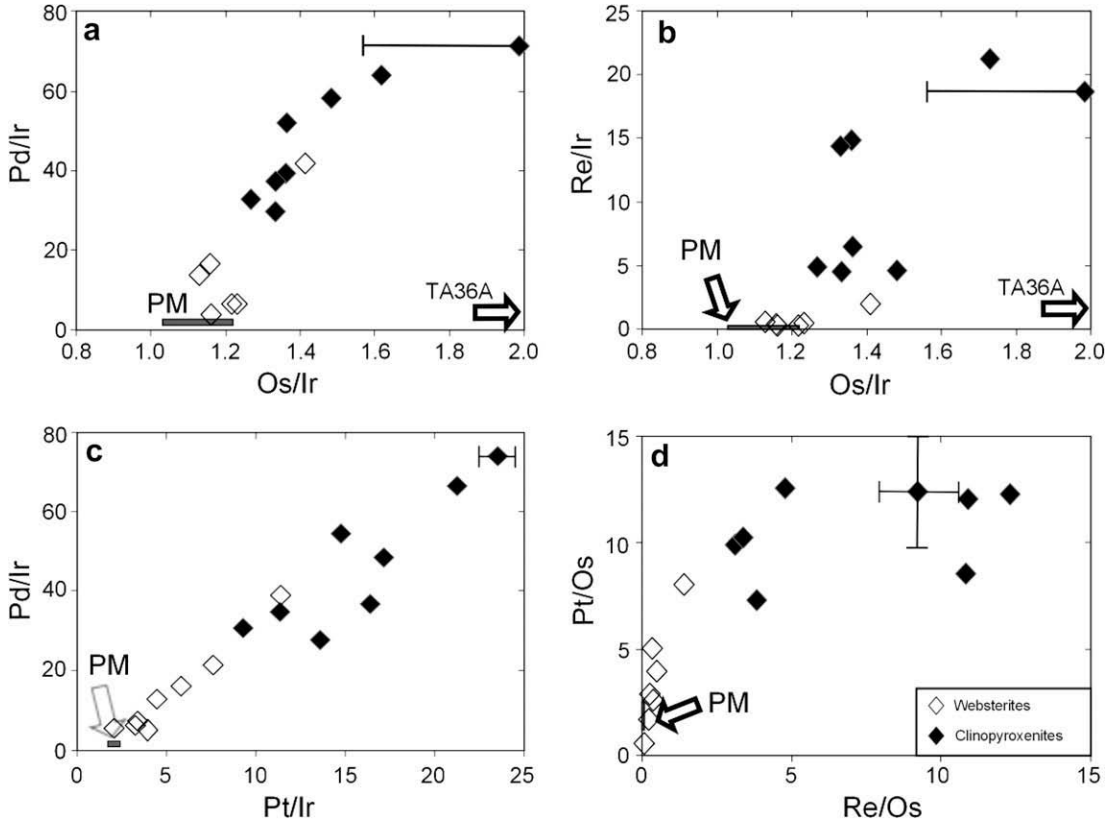

Fig. 10. (a–d) Plots of HSE inter-element ratios; PM: primitive mantle estimate (Becker et al., 2006); TA36A not plotted in (a) and (b) for scale reasons; open and filled symbols as in Fig. 1. Error bars are smaller than symbol size.

Sulfide grains of vastly different HSE compositions suggest disequilibrium on the sub-centimeter scale, as indicated by previous studies of sulfide populations in peridotites (Alard et al., 2000, 2002; Luguet et al., 2001, 2003, 2007; Lorand et al., 2008). Given that sulfides sited within 1 cm of each other may be in disequilibrium with respect to the HSE, single grain analyses of mantle sulfides may not be representative of the whole rock, especially for elements that show highly variable ratios such as Pd and Re. The heterogeneous distribution of HSE abundances, as well as the difficulty in identifying a Pt carrier phase, testifies to the difficulty of obtaining reliable mass balance constraints for the HSE on the basis of mineral compositions.

5.2. Websterite and clinopyroxenite formation

As demonstrated above, Totalp pyroxenites and their parental melts likely underwent a complex history of melting and mineral precipitation. Broad correlations of HSE with lithophile elements (Figs. 2 and 3) suggest coupled behavior of the HSE and lithophile elements. Totalp pyroxenites show both pyroxene macro- and megacryst cumulate textures and pyroxene clusters, interpreted to reflect remnants of trapped melt. Petrographic evidence from modally layered pyroxenites of several dm thickness (e.g. samples TA54, TA55) shows that websterites typically occur adjacent to peridotites, sometimes forming a 'boundary' between peridotite and clinopyroxenite similar to observations from other studies (Bodinier et al., 1987; Kornprobst et al., 1990; Garrido and Bodinier, 1999; Becker et al., 2004).

These observations along with geochemical characteristics are most easily explained by open-system interaction of olivine-undersaturated melt with wall rock peridotite and precipitation of high-Al pyroxene, garnet, and occasionally spinel near the garnet–spinel peridotite transition to form pyroxenites (O'Hara, 1968). Both websterites and clinopyroxenites would, thus, represent strongly melt-influenced systems. While websterites represent products of melt–rock interaction at lower melt/peridotite ratios, clinopyroxenites can be considered melt-dominated systems with high melt/peridotite ratios, in accordance with their HSE signatures (Figs. 6, 9 and 10) and high abundances of moderately incompatible elements such as Ca and Al. This model is supported by HSE heterogeneity observed in sulfides in samples TA11A2 and TA54A, especially for the mobile HSE Pd and Re. Variation in initial γ_{Os} in clinopyroxenites suggests the presence of at least two different melt endmembers with very radiogenic Os isotopic compositions (Fig. 6). Differences in initial γ_{Os} may reflect different extent of interaction of parental melts with peridotite, differences in age of the pyroxenites, or differences in age and Re/Os of the sublithospheric mantle source of the parental melts. Reaction of early-formed websterites with further batches of mafic melt and concurrent precipitation of pyroxenes and sulfide is proposed to result in the generation of Al-rich clinopyroxenites, in accordance with model calculations above (Fig. 9c), effectively shielding most of the reacting melt from direct contact with the host peridotite.

5.3. HSE composition of parental melts

As sulfides in Totalp websterites are in disequilibrium with each other, and may reflect at least partially compositions inherited from peridotite, HSE compositions of melts parental to the websterites are difficult to estimate. Sulfides from clinopyroxenites may display compositions closer to melt composition, but were not analyzed in this study because of their small size (<20 μm). Lithophile element compositions and radiogenic initial γ_{Os} indicate that bulk rock HSE compositions of Ca–Al-rich clinopyroxenites may approximate melt compositions. While the mostly subparallel patterns suggest similar relative abundances of the HSE in melts parental to the clinopyroxenites (Fig. 4, particularly samples TA 54 B to D), the behavior of Re warrants special attention. Sulfide-silicate partitioning coefficients for Re are substantially lower than for all other HSE, and are dependent on oxygen fugacity and silicate phase composition more than other HSE, and thus may also be controlled by silicate phases (Righter and Hauri, 1998; Righter et al., 2004; Mallmann and O'Neill, 2007). Re/Ir values in the websteritic sulfides of the present study cover a range from chondritic to about two orders of magnitude higher. Whole rock values in the websterites vary not quite as much, about a factor of 20. A rough mass balance for Re in websterites TA11A1 and TA54A using Re and sulfur abundances in whole rocks from Table 1 and median Re abundances in sulfides from Table 3 indicates that sulfides contain a large fraction of Re in these samples.

In summary, Totalp websterites contain sulfides that likely precipitated along with pyroxenes from infiltrating melts. Other sulfides in the websterites display Os/Ir or Ru/Ir similar to peridotites, but either Re/Ir or Pd/Ir are suprachondritic. This can be best explained if these sulfides have formed from hybrid melts containing larger quantities of peridotite-derived Os, Ir and Ru, as witnessed by the whole rock concentrations of these elements and the moderately radiogenic initial γ_{Os} (up to +28). Elevated Pt, Pd and Re contents in websterites and particularly in Al-rich clinopyroxenites are consistent with precipitation of sulfides from multiple melt batches. The clinopyroxenites apparently contain no peridotite-derived component and are dominated by the HSE signature of the mafic melts from which they precipitated. This interpretation is also supported by the highly radiogenic initial γ_{Os} values of as high as +1700.

5.4. Pyroxenites and the ^{186}Os–^{187}Os systematics of mantle rocks

Coupled suprachondritic $^{187}Os/^{188}Os$ and $^{186}Os/^{188}Os$ have been reported for several mantle-plume derived picritic and komatiitic lavas (Walker et al., 1997; Brandon et al., 1998, 1999, 2003; Brandon and Walker, 2005). Such coupled radiogenic isotope compositions require long-term isolation of a source with appropriate suprachondritic Re/Os and Pt/Os. Furthermore, long-term isolation is required, because of the low abundance and long half-life of ^{190}Pt, the parent isotope of ^{186}Os

(^{190}Pt: 0.0129%, $\lambda = 1.542 \times 10^{-12}$ a^{-1}; Begemann et al., 2001). Entrainment of approximately 0.5% of outer core material with suprachondritic ^{187}Os/^{188}Os and ^{186}Os/^{188}Os into the source of these mantle plumes has been proposed as a viable model (Walker et al., 1997; Brandon et al., 1998, 2003, 2006; Bird et al., 1999; Brandon and Walker, 2005). However, several studies pointed out problems with a significant core contribution to the lowermost mantle to explain observed Os isotope characteristics: a young age of the inner core based on core-mantle heat flow considerations (Lassiter, 2006), the absence of ^{182}W anomalies in the same samples (Scherstén et al., 2004), and new experimental results on high-pressure partitioning of Os, Re and Pt between liquid and solid Fe metal (Van Orman et al., 2008). In a recent study, Luguet et al. (2008) suggested that pyroxenite-derived sulfides can show the appropriate Pt–Re fractionations, and may evolve coupled ^{187}Os/^{188}Os–^{186}Os/^{188}Os systematics similar to that observed in some picrites and komatiites. The present study represents a substantial addition to the limited HSE database on pyroxenites, thus the feasibility of pyroxenites as contributing sources for plume-de-

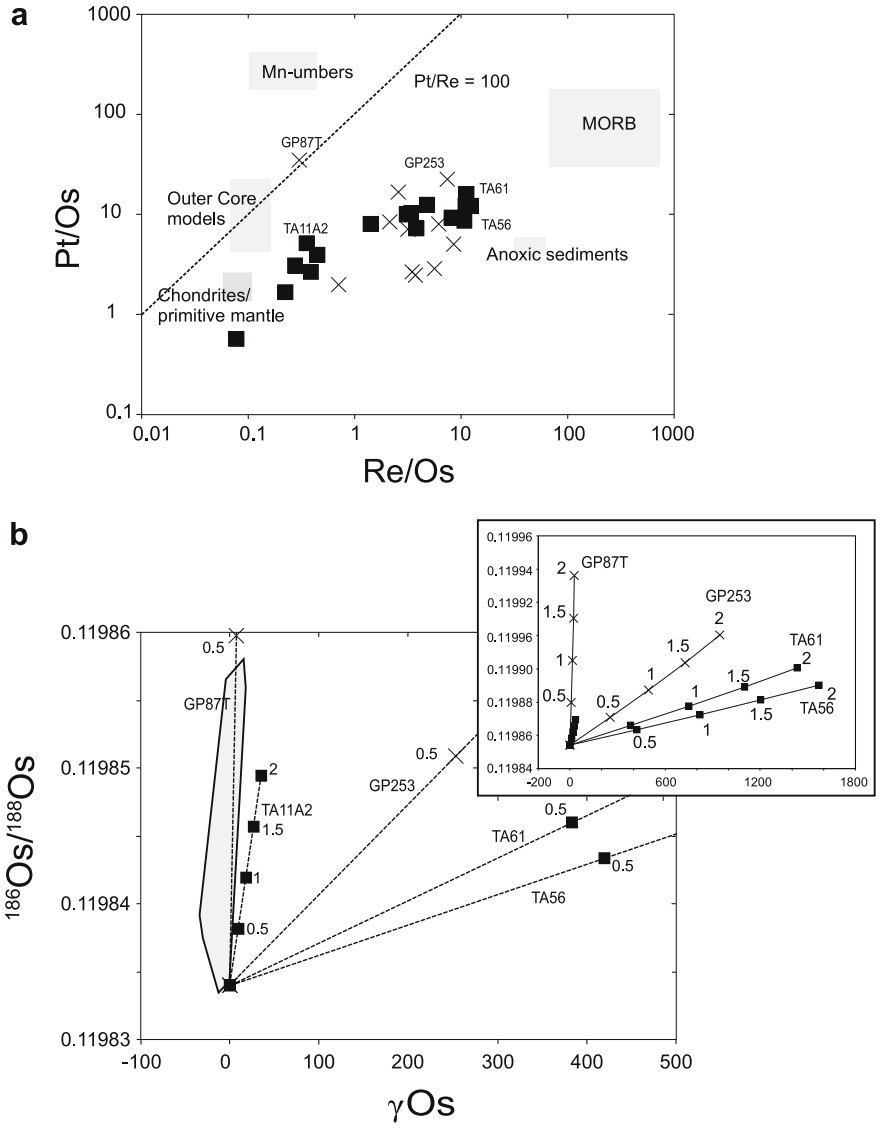

Fig. 11. (a) Pt/Os vs. Re/Os; squares: Totalp samples; crosses: Beni Bousera bulk rock pyroxenites from Luguet et al. (2008). Chondrite values from Horan et al. (2003); Primitive mantle from McDonough and Sun (1995), Walker et al. (1997) and Becker et al. (2006); Outer Core models from Brandon et al. (2003); Mn-umbers from Ravizza et al. (2001); MORB from Escrig et al. (2005) and Bézos et al. (2005); Reducing sediments from Ravizza and Pyle (1997) and Poirier (2006); (b) ^{186}Os/^{188}Os vs. γ_{Os}; shaded area: Hawaiian, Gorgona Island and Siberian samples from Brandon et al. (1999, 2003); lines represent isotopic evolution of pyroxenite samples from Totalp and Beni Bousera over time from chondritic values over 2 Ga; dotted lines: development of Beni Bousera samples GP87T and GP253 (Luguet et al., 2008) and TA11A2, TA56 and TA61 (this study). Most studied pyroxenites in both this study and Luguet et al. (2008) have too low Pt/Re and develop radiogenic ^{187}Os/^{188}Os too rapidly compared to ^{186}Os/^{188}Os to account for observed Os isotopic systematics attributed to core-mantle interaction. Therefore, mixing of a source containing these or similar pyroxenites and depleted mantle cannot reproduce the Hawaiian–Siberian trend of Brandon and Walker (2005).

rived lavas with suprachondritic ^{186}Os–^{187}Os systematics will be discussed here.

Pyroxenites from the Totalp massif show radiogenic initial $^{187}Os/^{188}Os$ coupled with chondritic to strongly suprachondritic Re/Os between 0.08 and 12.8, and Pt/Os between 0.57 and 15.9 (Fig. 11a). The variations of both ratios are within the range reported for both whole rock pyroxenites and sulfides from pyroxenites from Beni Bousera reported by Luguet et al. (2008). Pt/Re ratios of the whole rocks range between 0.79 and 14.8, well within the range reported by Luguet et al. (2008) for Beni Bousera pyroxenites. Thus, Totalp pyroxenites have strongly suprachondritic Re/Os and Pt/Os and will, with time, produce elevated $^{187}Os/^{188}Os$ and $^{186}Os/^{188}Os$, relative to chondrites. However, in order to match the coupled suprachondritic $^{187}Os/^{188}Os$–$^{186}Os/^{188}Os$ data observed in picrites from Hawaii, Brandon et al. (1999) calculated a required Pt/Re of ~88–100. Such high Pt/Re values are reported for only a few pyroxenite whole rocks or pyroxenite hosted sulfides (this study, Fig. 11a; Luguet et al., 2008). The majority of pyroxenite samples for which HSE data are available, will develop radiogenic $^{187}Os/^{188}Os$ too rapidly (Fig. 11b). Mixtures of fertile lherzolitic mantle and most pyroxenite compositions cannot explain the range from chondritic to suprachondritic Os isotopic ratios in Hawaiian picrites and Gorgona komatiites (e.g. Brandon and Walker (2005). Another problem is related to the low-Os concentrations of many pyroxenites. To reproduce radiogenic $^{186}Os/^{188}Os$ observed in picrites by a mixed pyroxenite-peridotite source, the amount of pyroxenite in the melt source and thus, by inference, recycled crust needs to be as high as 90%. Although this estimate is strongly dependent on the pyroxenite composition, it may be unreasonably large (Walker et al., 1994, 1997; Luguet et al., 2008; Dale et al., 2009).

Some base metal sulfides and Pt-rich alloys from eclogite, pyroxenites or ophiolites have the appropriate Pt/Re ratios (Luguet et al., 2008) to produce the observed coupled $^{187}Os/^{188}Os$–$^{186}Os/^{188}Os$ systematics after sufficient isolation time. How representative such compositions are for samples on the scale of hand specimen or even larger mantle domains, however, remains an important open question. The heterogeneity in sulfide and alloy compositions and the contrasts with bulk rock HSE compositions of pyroxenites reported here and in a variety of peridotites elsewhere (e.g. Alard et al., 2000, 2002) indicate that the mass balance of such phases must be well constrained before extrapolations to whole rock compositions or even larger scale processes can be considered reliable.

6. CONCLUSIONS

Modeling results suggest that pyroxenites of the Totalp ultramafic massif formed as cumulates from melts reacting to various extents with mantle peridotites in the spinel lherzolite facies, as suggested for other pyroxenite suites (Obata, 1980; Sinigoi et al., 1983; Bodinier et al., 1987, 1990; Takahashi, 1992; Davies et al., 1993; Pearson et al., 1993; Vaselli et al., 1995; Becker, 1996; Kumar et al., 1996; Garrido and Bodinier, 1999). Cumulate precipitation of sulfides bearing a melt signature is required to account for high Pt, Pd and Re concentrations and HSE fractionations observed (e.g. Rehkämper et al., 1999b). While the websterites precipitated from hybrid melts derived from reaction of small amounts of externally derived melt with peridotite, clinopyroxenites may have formed in a melt-dominated system by limited reaction of existing websterites with further batches of pyroxene-saturated melt, thus acquiring the HSE and radiogenic Os isotope signature of the melts. Multiple melt batches derived from reservoirs with suprachondritic, but disparate Re/Os and $^{187}Os/^{188}Os$ are required to account for the variably radiogenic initial $^{187}Os/^{188}Os$ of Al-rich clinopyroxenites.

The Pd and Re rich nature and radiogenic Os isotopic composition of Totalp pyroxenites are consistent with derivation of parental melts by partial melting of mafic components in the convecting mantle. Sulfide melt–mss partitioning of the HSE during partial melting of subducted oceanic crust can only generate appropriate HSE fractionations in partial melts if mss is stable in the source rocks. The variations in HSE abundances and their patterns are a complex function of variable degree of melting, melt–rock reactions, and variable melt source composition. In the present case, an origin as in situ melts of wall rock peridotite or as residues from partial melting of slices of recycled oceanic crust appears unlikely.

Pyroxenites or their sulfides as a source of plume-related lavas with high $^{186}Os/^{188}Os$ and $^{187}Os/^{188}Os$ remain a problematic proposition. While some base metal sulfides and Pt-rich alloys have sufficiently high Pt/Re to produce high $^{186}Os/^{188}Os$ and $^{187}Os/^{188}Os$ signatures over time (Luguet et al., 2008), small scale HSE heterogeneities in pyroxenites cast doubt on the representativeness of these analyses. Based on whole rock HSE compositions, by far most pyroxenites in the present study and others have too little Os and are too enriched in Re compared to Pt to account for the coupled ^{186}Os- and ^{187}Os-enriched isotopic ratios observed in some mantle melts.

ACKNOWLEDGMENTS

We thank C. Behr, M. Feth, H. Frohna-Binder, A. Gottsche, K. Hammerschmidt, W. Michaelis, R. Milke, R. Naumann, B. Pracejus and I. Puchtel for technical assistance. Sulfur analyses at the University of Leicester were provided by the late Dr. T.S. Brewer. The electron microprobe analyses were performed in the NispLab and we acknowledge the support of the Maryland Nano-Center and its NispLab. Discussions with J.-P. Lorand, S.J. Barnes, V. Le Roux, A.J.V. Riches and O. Müntener are gratefully acknowledged. We thank Chris Dale, Olivier Alard, an anonymous reviewer and Mark Rehkämper (associate editor) for comments and editorial handling which significantly improved the manuscript. This work was partly funded by NSF Grant EAR 0309810 to H.B. and R.J.W. and EAR 0739006 to W.F.M. and funds from the Freie Universität Berlin.

APPENDIX A. SUPPLEMENTARY DATA

Supplementary data associated with this article can be found, in the online version, at doi:10.1016/j.gca.2009.10.007.

REFERENCES

Alard O., Griffin W. L., Lorand J.-P., Jackson S. E. and O'Reilly S. Y. (2000) Non-chondritic distribution of the highly siderophile elements in mantle sulphides. *Nature* **407**, 891–894.

Alard O., Griffin W. L., Pearson N. J., Lorand J.-P. and O'Reilly S. Y. (2002) New insights into the Re–Os systematics of sub-continental lithospheric mantle from in situ analysis of sulphides. *Earth Planet. Sci. Lett.* **203**, 651–663.

Allègre C. J. and Turcotte D. L. (1986) Implications of a two-component marble-cake mantle. *Nature* **323**, 123–127.

Amossé J., Dablé P. and Allibert M. (2000) Thermochemical behaviour of Pt, Ir, Rh and Ru vs. fO_2 and fS_2 in a basaltic melt. Implications for the differentiation and precipitation of these elements. *Mineral. Petrol.* **68**, 29–62.

Andrews D. R. A. and Brenan J. M. (2002) The solubility of ruthenium in sulfide liquid: implications for platinum group mineral stability and sulfide melt–silicate melt partitioning. *Chem. Geol.* **192**, 163–181.

Aulbach S., Creaser R. A., Pearson N. J., Simonetti S. S., Heaman L. M., Griffin W. L. and Stachel T. (2009) Sulfide and whole rock Re–Os systematics of eclogite and pyroxenite xenoliths from the Slave Craton, Canada. *Earth Planet. Sci. Lett.* **283**, 48–58.

Ballhaus C., Tredoux M. and Späth A. (2001) Phase relations in the Fe–Ni–Cu–PGE–S system at magmatic temperature and application to massive sulphide ores of the sudbury igneous complex. *J. Petrol.* **42**, 1911–1926.

Ballhaus C., Bockrath C., Wohlgemuth-Ueberwasser C., Laurenz V. and Berndt J. (2006) Fractionation of the noble metals by physical processes. *Contrib. Mineral. Petrol.* **152**, 667–684.

Barnes S. J. (1993) Partitioning of the platinum group elements and gold between silicate and sulphide magmas in the Munni Munni complex, Western Australia. *Geochim. Cosmochim. Acta* **57**, 1277–1290.

Becker H. (1996) Crustal trace element and isotopic signatures in garnet pyroxenites from garnet peridotite massifs from lower Austria. *J. Petrol.* **37**, 785–810.

Becker H. (2000) Re–Os fractionation in eclogites and blueshists and the implications for recycling of oceanic crust into the mantle. *Earth Planet. Sci. Lett.* **177**, 287–300.

Becker H., Carlson R. W. and Shirey S. B. (2004) Slab-derived osmium and isotopic disequilibrium in garnet pyroxenites from a Paleozoic convergent plate margin (lower Austria). *Chem. Geol.* **208**, 141–156.

Becker H., Horan M. F., Walker R. J., Gao S., Lorand J.-P. and Rudnick R. L. (2006) Highly siderophile element composition of the Earth's primitive upper mantle: constraints from new data on peridotite massifs and xenoliths. *Geochim. Cosmochim. Acta* **70**, 4528–4550.

Begemann F., Ludwig K. R., Lugmair G. W., Nyquist L. E., Patchett P. J., Renne P. R., Shih C.-Y., Villa I. M. and Walker R. J. (2001) Call for an improved set of decay constants for geochronological use. *Geochim. Cosmochim. Acta* **65**(1), 111–121.

Bezmen N. I., Asif M., Brügmann G., Romanenko I. M. and Naldrett A. J. (1994) Distribution of Pd, Rh, Ru, Ir, Os and Au between sulfide and silicate metals. *Geochim. Cosmochim. Acta* **58**, 1251–1260.

Bézos A., Lorand J.-P., Humler E. and Gros M. (2005) Platinum-group element systematics in Mid-Oceanic Ridge basaltic glasses from the Pacific, Atlantic and Indian Oceans. *Geochim. Cosmochim. Acta* **69**(10), 2613–2627.

Birck J.-L., Roy-Barman M. and Capmas F. (1997) Os isotopic measurements at the femtomole level in natural samples. *Geostand. Newsl.*(1), 19–27.

Bird J. M., Meibom A., Frei R. and Nägler T. F. (1999) Osmium and lead isotopes of rare OsIrRu minerals: derivation from the core-mantle boundary region? *Earth Planet. Sci. Lett.* **170**, 83–92.

Blichert-Toft J., Albarède F. and Kornprobst J. (1999) Lu–Hf isotope systematics of garnet pyroxenites from Beni Bousera, Morocco: implications for basalt origin. *Science* **283**, 1303–1306.

Blusztajn J., Hart S. R., Ravizza G. E. and Dick H. J. B. (2000) Platinum-group elements and Os isotope characteristics of the lower oceanic crust. *Chem. Geol.* **168**, 113–122.

Bockrath C., Ballhaus C. and Holzheid A. (2004) Fractionation of the platinum-group elements during mantle melting. *Science* **305**, 1951–1953.

Bodinier J. L. (1988) Geochemistry and petrogenesis of the Lanzo peridotite body, western Alps. *Tectonophysics* **149**, 67–88.

Bodinier J. L. and Godard M. (2003) Orogenic, ophiolitic, and abyssal peridotites. In *Treatise on Geochemistry, Part 2*, vol. 2 (eds. K. K. Turekian and H. D. Holland). Elsevier Ltd., Amsterdam, The Netherlands, pp. 103–170.

Bodinier J. L., Guiraud M., Fabriès J., Dostal J. and Dupuy C. (1987) Petrogenesis of layered pyroxenites from the Lherz, Freychinède and Prades ultramafic bodies (Ariège, french Pyrénées). *Geochim. Cosmochim. Acta* **51**, 279–290.

Bodinier J. L., Vasseur G., Vernieres J., Dupuy C. and Fabries J. (1990) Mechanisms of mantle metasomatism: geochemical evidence from the lherz orogenic peridotite. *J. Petrol.* **31**(3), 597–628.

Brandon A. D. and Walker R. J. (2005) The debate over core-mantle interaction. *Earth Planet. Sci. Lett.* **232**, 211–225.

Brandon A. D., Walker R. J., Morgan J. W., Norman M. D. and Prichard H. M. (1998) Coupled ^{186}Os and ^{187}Os evidence for core–mantle interaction. *Science* **280**, 1570–1573.

Brandon A. D., Norman M. D., Walker R. J. and Morgan J. W. (1999) ^{186}Os–^{187}Os systematics of Hawaiian picrites. *Earth Planet. Sci. Lett.* **174**, 25–42.

Brandon A. D., Walker R. J., Puchtel I. S., Becker H., Humayun M. and Revillon S. (2003) ^{186}Os–^{187}Os systematics of Gorgona Island komatiites: implications for early growth of the inner core. *Earth Planet. Sci. Lett.* **206**, 411–426.

Brandon A. D., Walker R. J. and Puchtel I. S. (2006) Platinum–osmium isotope evolution of the Earth's mantle: constraints from chondrites and Os-rich alloys. *Geochim. Cosmochim. Acta* **70**, 2093–2103.

Brenan J. M. (2002) Re–Os fractionation in magmatic sulfide melt by monosulfide solid solution. *Earth Planet. Sci. Lett.* **199**, 257–268.

Brenan J. M. (2008) Re–Os fractionation by sulfide melt–silicate melt partitioning: a new spin. *Chem. Geol.* **248**, 140–165.

Campbell I. H. and Naldrett A. J. (1979) The influence of silicate: sulfide ratios on the geochemistry of magmatic sulfides. *Econ. Geol.* **74**(6), 1503–1506.

Cohen A. S. and Waters F. G. (1996) Separation of osmium from geological materials by solvent extraction for analysis by thermal ionization mass spectrometry. *Anal. Chim. Acta* **332**, 269–275.

Dale C. W., Gannoun A., Burton K. W., Argles T. W. and Parkinson I. J. (2007) Rhenium–osmium isotope and elemental behaviour during subduction of oceanic crust and the implications for mantle recycling. *Earth Planet. Sci. Lett.* **253**, 211–225.

Dale C. W., Luguet A., MacPherson G. J., Pearson D. G. and Hickey-Vargas R. (2008) Extreme platinum-group element fractionation and variable Os isotope compositions in Philippine Sea Plate basalts: tracing mantle source heterogeneity. *Chem. Geol.* **248**, 213–238.

Dale C. W., Burton K. W., Pearson D. G., Gannoun A., Alard O., Argles T. W. and Parkinson I. J. (2009) Highly siderophile element behaviour accompanying subduction of oceanic crust: whole rock and mineral-scale insights from a high-pressure terrain. *Geochim. Cosmochim. Acta* **73**, 1394–1416.

Dantas C., Ceuleneer G., Grégoire M., Python M., Freydier R., Warren J. and Dick H. J. B. (2007) Pyroxenites from the Southwest Indian Ridge, 9–16 E: cumulates from incremental melt fractions produced at the top of a cold melting regime. *J. Petrol.* **48**(4), 647–660.

Davies G. R., Nixon P. H., Pearson D. G. and Obata M. (1993) Tectonic implications of graphitized diamonds from the Ronda peridotite massif, southern Spain. *Geology* **21**(5), 471–474.

Desmurs L., Müntener O. and Manatschal G. (2002) Onset of magmatic accretion within a magma-poor rifted margin: a case study from the Platta ocean-continent transition, eastern Switzerland. *Contrib. Mineral. Petrol.* **144**, 365–382.

Dick H. J. B. and Sinton J. M. (1979) Compositional layering in alpine peridotites: evidence for pressure solution creep in the mantle. *J. Geol.* **87**, 403–416.

Dick H. J. B., Lin J. and Schouten H. (2003) An ultraslow-spreading class of ocean ridge. *Nature* **426**, 405–412.

Downes H. (2007) Origin and significance of spinel and garnet pyroxenites in the shallow lithospheric mantle: ultramafic massifs in orogenic belts in Western Europe and NW Africa. *Lithos* **99**, 1–24.

Downes H., Bodinier J.-L., Thirlwall M. F., Lorand J.-P. and Fabries J. (1991) REE and Sr–Nd isotopic geochemistry of Eastern Pyrenean peridotite massifs: sub-continental lithospheric mantle modified by continental magmatism. *J. Petrol. Spec. Lherzolite Issue*, 97–115.

Escrig S., Schiano P., Schilling J.-G. and Allègre C. J. (2005) Rhenium–osmium isotope systematics in MORB from the Southern Mid-Atlantic Ridge (40–50 S). *Earth Planet. Sci. Lett.* **235**, 528–548.

Fleet M. E., Chryssoulis S. L., Stone W. E. and Weisener C. G. (1993) Partitioning of platinum-group elements and Au in the Fe–Ni–Cu–S system: experiments on the fractional crystallization of sulfide melt. *Contrib. Mineral. Petrol.* **115**, 36–44.

Fleet M. E., Crocket J. H., Liu M. and Stone W. E. (1999) Laboratory partitioning of platinum-group elements (PGE) and gold with application to magmatic sulfide-PGE deposits. *Lithos* **47**, 127–142.

Fonseca R. O. C., Mallmann G., O'Neill H. S. C. and Campbell I. H. (2007) How chalcophile is rhenium? An experimental study of the solubility in sulphide mattes. *Earth Planet. Sci. Lett.* **260**, 537–548.

Früh-Green G., Weissert H. and Bernoulli D. (1990) A multiple fluid history recorded in Alpine ophiolites. *J. Geol. Soc.* **147**, 959–970.

Gannoun A., Burton K. W., Parkinson I. J., Alard O., Schiano P. and Thomas L. E. (2007) The scale and origin of the osmium isotope variations in mid-ocean ridge basalts. *Earth Planet. Sci. Lett.* **259**, 541–556.

Garrido C. J. and Bodinier J. L. (1999) Diversity of mafic rocks in the ronda peridotite: evidence for pervasive melt–rock reaction during heating of subcontinental lithosphere by upwelling asthenosphere. *J. Petrol.* **40**(5), 729–754.

Garuti G., Gorgoni C. and Sighinolfi G. P. (1984) Sulfide mineralogy and chalcophile and siderophile element abundances in the Ivrea-Verbano mantle peridotites (Western Italian Alps). *Earth Planet. Sci. Lett.* **70**, 69–87.

Greau Y., Griffin W. L., Alard O. and O'Reilly S. Y. (2008) Petrology and geochemistry of eclogitic sulfides: a new insight on the origin of mantle eclogites. In *9th International Kimberlite Conference*, Frankfurt, Germany. No. 91KC-A-000126.

Hart S. R. and Ravizza G. E. (1996) Os partitioning between phases in lherzolite and basalt. In *Earth Processes: Reading the Isotopic Code*, vol. 95 (eds. A. Basu and S. Hart). American Geophysical Union, pp. 123–134.

Haughton D. R., Roeder P. L. and Skinner B. J. (1974) Solubility of sulfur in mafic magmas. *Econ. Geol.* **69**(4), 451–467.

Hirschmann M. M. and Stolper E. M. (1996) A possible role for garnet pyroxenite in the origin of the "garnet signature" in MORB. *Contrib. Mineral. Petrol.* **124**, 185–208.

Hirschmann M. M., Kogiso T., Baker M. B. and Stolper E. M. (2003) Alkalic magmas generated by partial melting of garnet pyroxenite. *Geology* **31**, 481–484.

Holzheid A. and Grove T. L. (2002) Sulfur saturation limits in silicate melts and their implications for core formation scenarios for terrestrial planets. *Am. Mineral.* **87**, 227–237.

Horan M. F., Walker R. J., Morgan J. W., Grossman J. N. and Rubin A. E. (2003) Highly siderophile elements in chondrites. *Chem. Geol.* **196**, 5–20.

Irving A. J. (1980) Petrology and geochemistry of composite ultramafic xenoliths in alakaic basalts and implications for magmatic processes within the mantle. *Am. J. Sci.* **280A**, 389–426.

Kogiso T., Hirschmann M. M. and Frost D. J. (2003) High pressure partial melting of garnet pyroxenite: possible mafic lithologies in the source of ocean island basalts. *Earth Planet. Sci. Lett.* **216**, 603–617.

Kogiso T., Hirschmann M. M. and Pertermann M. (2004) High-pressure partial melting of mafic lithologies in the mantle. *J. Petrol.* **45**(12), 2407–2422.

Kornprobst J. (1969) Le massif ultrabasique des Beni Bouchera (Rif Interne, Maroc): etude des péridotites de haute température et de haute pression, et des pyroxénolites, à grenat ou sans grenat, qui leur sont associées. *Contrib. Mineral. Petrol.* **23**, 283–322.

Kornprobst J., Piboule M., Roden M. F. and Tabit A. (1990) Corundum-bearing garnet clinopyroxenites at Beni Bousera (Morocco): original plagioclase-rich gabbros recrystallized at depth within the mantle? *J. Petrol.* **31**(3), 717–745.

Kumar N., Reisberg L. and Zindler A. (1996) A major and trace element and strontium, neodymium, and osmium isotopic study of a thick pyroxenite layer from the Beni Bousera Ultramafic Complex of northern Morocco. *Geochim. Cosmochim. Acta* **60**(8), 1429–1444.

Lagabrielle Y. and Lemoine M. (1997) Alpine, corsican and Apennine ophiolites: the slow-spreading ridge model. *C. R. Acad. Sci. Paris, Sci. Terre Planètes* **325**, 909–920.

Lassiter J. C. (2006) Constraints on the coupled thermal evolution of the Earth's core and mantle, the age of the inner core, and the origin of the $^{186}Os/^{188}Os$ "core signal" in plume-derived lavas. *Earth Planet. Sci. Lett.* **250**, 306–317.

Lassiter J. C., Hauri E. H., Reiners P. W. and Garcia M. O. (2000) Generation of Hawaiian post-erosional lavas by melting of a mixed lherzolite/pyroxenite source. *Earth Planet. Sci. Lett.* **178**, 269–284.

Lee C.-T. A., Brandon A. D. and Norman M. (2003) Vanadium in peridotites as a proxy for paleo-fO_2 during partial melting: prospects, limitations, and implications. *Geochim. Cosmochim. Acta* **67**(16), 3045–3064.

Li C., Barnes S.-J., Makovicky E., Rose-Hansen J. and Makovicky M. (1996) Partitioning of nickel, copper, iridium, rhenium, platinum and palladium between monosulfide solid solution and sulfide liquid: effects of composition and temperature. *Geochim. Cosmochim. Acta* **60**(7), 1231–1238.

Liu Y., Samaha N.-T. and Baker D. R. (2007) Sulfur concentration at sulfide saturation (SCSS) in magmatic silicate melts. *Geochim. Cosmochim. Acta* **71**, 1783–1799.

Lorand J.-P. (1989) Abundance and distribution of Cu–Fe–Ni sulfides, sulfur, copper and platinum-group elements in orogenic-type spinel lherzolite massifs of Ariège (northeastern Pyrenees, France). *Earth Planet. Sci. Lett.* **93**, 50–64.

Lorand J.-P., Luguet A., Alard O., Bézos A. and Meisel T. (2008) Abundance and distribution of platinum-group in orogenic lherzolites; a case study in a Fontete Rouge lherzolite (French Pyrénées). *Chem. Geol.* **248**, 174–194.

Loubet M. and Allègre C. J. (1982) Trace elements in orogenic lherzolites reveal the complex history of the upper mantle. *Nature* **298**, 809–814.

Luguet A. and Lorand J.-P. (1999) Minéralogie des sulfures des Fe–Ni–Cu dans les péridotites abyssales de la zone Mark (ride Médio-Atlantique, 20–24 N). *C. R. Acad. Sci. Paris, Sci. Terre Planètes* **329**, 637–644.

Luguet A., Alard O., Lorand J.-P., Pearson N. J., Ryan C. and O'Reilly S. Y. (2001) Laser-ablation microprobe (LAM)-ICPMS unravels the highly siderophile element geochemistry of the oceanic mantle. *Earth Planet. Sci. Lett.* **189**, 285–294.

Luguet A., Lorand J.-P. and Seyler M. (2003) Sulfide petrology and highly siderophile element geochemistry of abyssal peridotites: a coupled study of samples from the Kane Fracture Zone (45 W 23 20 N, MARK Area, Atlantic Ocean). *Geochim. Cosmochim. Acta* **67**(8), 1553–1570.

Luguet A., Shirey S. B., Lorand J.-P., Horan M. F. and Carlson R. W. (2007) Residual platinum-group minerals from highly depleted harzburgites of the Lherz massif (France) and their role in HSE fractionation of the mantle. *Geochim. Cosmochim. Acta* **71**, 3082–3097.

Luguet A., Pearson D. G., Nowell G. N., Dreher S. T., Coggon J. A., Spetsius Z. V. and Parman S. W. (2008) Enriched Pt–Re–Os isotope systematics in plume lavas explained by metasomatic sulfides. *Science* **319**, 453–456.

Mallmann G. and O'Neill H. S. C. (2007) The effect of oxygen fugacity on the partitioning of Re between crystals and silicate melt during mantle melting. *Geochim. Cosmochim. Acta* **71**, 2837–2857.

Manatschal G. and Bernoulli D. (1998) Rifting and early evolution of ancient ocean basins: the record of the Mesozoic Tethys and of the Galicia-Newfoundland margins. *Mar. Geophys. Res.* **20**, 371–381.

Mavrogenes J. A. and O'Neill H. S. C. (1999) The relative effects of pressure, temperature and oxygen fugacity on the solubility of sulfide in mafic magmas. *Geochim. Cosmochim. Acta* **63**(7/8), 1173–1180.

McDonough W. F. and Sun S.-S. (1995) The composition of the Earth. *Chem. Geol.* **120**, 223–253.

Meisel T., Fellner N. and Moser J. (2003) A simple procedure for the determination of platinum group elements and rhenium (Ru, Rh, Pd, Re, Os, Ir and Pt) using ID-ICP-MS with an inexpensive on-line matrix separation in geological and environmental materials. *J. Anal. At. Spectrom.* **18**, 720–726.

Melcher F. and Meisel T. (2004) A metamorphosed early cambrian crust-mantle transition in the eastern Alps, Austria. *J. Petrol.* **45**(8), 1689–1723.

Michael P. J., Langmuir C. H., Dick H. J. B., Snow J. E., Goldstein S. L., Graham D. W., Lehnert K., Kurras G., Jokat W., Mühe R. and Edmonds H. N. (2003) Magmatic and amagmatic seafloor generation at the ultraslow-spreading Gakkel ridge, Arctic Ocean. *Nature* **423**, 956–961.

Morgan J. W. and Lovering J. F. (1967) Rhenium and osmium abundances in some igneous and metamorphic rocks. *Earth Planet. Sci. Lett.* **3**, 219–224.

Morgan J. W., Wandless G. A., Petrie R. K. and Irving A. J. (1981) Composition of the Earth's upper mantle-I. Siderophile trace elements in ultramafic nodules. *Tectonophysics* **75**, 47–67.

Morishita T., Arai S., Gervilla F. and Green D. H. (2003) Closed-system geochemical recycling of crustal materials in alpine-type peridotite. *Geochim. Cosmochim. Acta* **67**(2), 303–310.

Mukasa S. B., Shervais J. W., Wilshire H. G. and Nielson J. E. (1991) Intrinsic Nd, Pb, and Sr Isotopic heterogeneities exhibited by the lherz Alpine peridotite massif, French Pyrenees. *J. Petrol. Spec. Lherzolite Issue* **117**, 134.

Mungall J. E., Andrews D. R. A., Cabri L. J., Sylvester P. J. and Tubrett M. (2005) Partitioning of Cu, Ni, Au and platinum-group elements between monosulfide solid solution and sulfide melt under controlled oxygen and sulfur fugacities. *Geochim. Cosmochim. Acta* **69**(17), 4349–4360.

Müntener O. and Hermann J. (2001) The role of lower crust and continental upper mantle during formation of non-volcanic passive margins: evidence from the Alps. In *Non-Volcanic Rifting of Continental Margins: A Comparison of Evidence from Land and Sea*, vol. 187 (eds. R. C. L. Wilson, R. B. Whitmarsh, B. Taylor and N. Froitzheim). Geological Society, pp. 267–288.

Müntener O., Pettke T., Desmurs L., Meier M. and Schaltegger U. (2004) Refertilization of mantle peridotite in embryonic ocean basins: trace element and Nd isotopic evidence and implications for crust-mantle relationships. *Earth Planet. Sci. Lett.* **221**, 293–308.

Obata M. (1980) The ronda peridotite: garnet-, spinel-, and plagioclase-lherzolite facies and the P–T-trajectories of a high-temperature mantle intrusion. *J. Petrol.* **21**(3), 533–572.

Obata M., Hirajima T. and Svojtka M. (2006) Origin of eclogite and garnet pyroxenite from the Moldanubian Zone of the Bohemian Massif, Czech Republic and its implication to other mafic layers embedded in orogenic peridotites. *Mineral. Petrol.* **88**, 321–340.

O'Hara M. J. (1968) The bearing of phase equilibria studies in synthetic and natural systems on the origin and evolution of basic and ultrabasic rocks. *Earth Sci. Rev.* **4**, 69–133.

O'Neill H. S. C. and Mavrogenes J. A. (2002) The sulfide capacity and the sulfur content at sulfide saturation of silicate melts at 1400 °C and 1 bar. *J. Petrol.* **43**(6), 1049–1087.

O'Reilly S. Y. and Griffin W. L. (1995) Trace-element partitioning between garnet and clinopyroxene in mantle-derived pyroxenites and eclogites: P–T–X controls. *Chem. Geol.* **121**, 105–130.

Peach C. L., Mathez E. A. and Keays R. R. (1990) Sulfide melt–silicate melt distribution coefficients for noble metals and other chalcophile elements as deduced from MORB: implications for partial melting. *Geochim. Cosmochim. Acta* **54**, 3379–3389.

Peach C. L., Mathez E. A., Keays R. R. and Reeves S. J. (1994) Experimentally determined sulfide melt–silicate melt partition coefficients for iridium and palladium. *Chem. Geol.* **117**, 361–377.

Pearson D. G. and Nowell G. N. (2004) Re–Os and Lu–Hf isotope constraints on the origin and age of pyroxenites from the Beni Bousera peridotite massif: implications for mixed peridotite–pyroxenite mantle sources. *J. Petrol.* **45**(2), 439–455.

Pearson D. G., Davies G. R. and Nixon P. H. (1993) Geochemical constraints on the petrogenesis of diamond facies pyroxenites from the Beni Bousera peridotite massif, North Morocco. *J. Petrol.* **34**(1), 125–172.

Pearson D. G., Irvine G. J., Ionov D. A., Boyd F. R. and Dreibus G. E. (2004) Re–Os isotope systematics and platinum group element fractionation during mantle melt extraction: a study of massif and xenolith peridotite suites. *Chem. Geol.* **208**, 29–59.

Pertermann M. and Hirschmann M. M. (2003) Partial melting experiments on a MORB-like pyroxenite between 2 and 3 GPa: Constraints on the presence of pyroxenite in basalt source regions from solidus location and melting rate. *J. Geophys. Res.* **108**(B2), 2125. doi:10.1029/2000JB000118.

Peters T. (1963) Mineralogie und petrographie des Totalpserpentins bei davos. *Schweiz. Mineral. Petrogr. Mitt.* **43**, 531–685.

Peters T. (1968) Distribution of Mg, Fe, Al, Ca and Na in coexisting olivine, orthopyroxene and clinopyroxene in the Totalp serpentinite (Davos, Switzerland) and in the Alpine metamorphosed malenco serpentinite (N. Italy). *Contrib. Mineral. Petrol.* **18**, 65–75.

Peters T. and Stettler A. (1987) Radiometric age, thermobarometry and mode of emplacement of the Totalp peridotite in the Eastern Swiss Alps. *Schweiz. Mineral. Petrogr. Mitt.* **67**, 285–294.

Piccardo G. B., Messiga B. and Vannucci R. (1988) The Zabargad peridotite-pyroxenite association: petrological constraints on evolution. *Tectonophysics* **150**, 135–162.

Piccardo G. B., Müntener O. and Zanetti A. (2004) Alpine–Apennine ophiolitic peridotites: new concepts on their composition and evolution. *Ofioliti* **29**(1), 63–74.

Poirier A. (2006) Re–Os and Pb isotope systematics in reduced fjord sediments from Saanich Inlet (Western Canada). *Earth Planet. Sci. Lett.* **249**, 119–131.

Polvé M. and Allègre C. J. (1980) Orogenic lherzolite complexes studied by ^{87}Rb–^{87}Sr: a clue to understand the mantle convection processes? *Earth Planet. Sci. Lett.* **51**, 71–93.

Pruseth K. L. and Palme H. (2004) The solubility of Pt in liquid Fe-sulfides. *Chem. Geol.* **208**, 233–245.

Rajamani V. and Naldrett A. J. (1978) Partitioning of Fe, Co, Ni and Cu between sulfide liquid and basaltic melts and the composition of Ni–Cu sulfide deposits. *Econ. Geol.* **73**, 83–92.

Rapp R. P. and Watson E. B. (1995) Dehydration melting of metabasalt at 8–32 kbar: implications for continental growth and crust-mantle recycling. *J. Petrol.* **36**(4), 891–931.

Ravizza G. and Pyle D. (1997) PGE and Os isotopic analyses of single sample aliquots with NiS fire assay preconcentration. *Chem. Geol.* **141**, 251–268.

Ravizza G., Blusztajn J. and Prichard H. M. (2001) Re–Os systematics and platinum-group element distribution in metalliferous sediments from the Troodos ophiolite. *Earth Planet. Sci. Lett.* **188**, 369–381.

Rehkämper M., Halliday A. N., Fitton G., Lee D.-C., Wieneke M. and Arndt N. T. (1999a) Ir, Ru, Pt, and Pd in basalts and komatiites: new constraints for the geochemical behavior of the platinum-group elements in the mantle. *Geochim. Cosmochim. Acta* **62**(22), 3915–3934.

Rehkämper M., Halliday A. N., Alt J., Fitton J. G., Zipfel J. and Takazawa E. (1999b) Non-chondritic platinum-group element ratios in oceanic mantle lithosphere: petrogenetic signature of melt percolation? *Earth Planet. Sci. Lett.* **172**, 65–81.

Richardson S. H., Shirey S. B., Harris J. W. and Carlson R. W. (2001) Archaean subduction recorded by Re–Os isotopes in eclogitic sulfide inclusions in Kimberley diamonds. *Earth Planet. Sci. Lett.* **191**, 257–266.

Righter K. and Hauri E. H. (1998) Compatibility of rhenium in garnet during mantle melting and magma genesis. *Science* **280**, 1737–1741.

Righter K., Campbell A. J., Humayun M. and Hervig R. L. (2004) Partitioning of Ru, Rh, Pd, Re, Ir, and Au between Cr-bearing spinel, olivine, pyroxene and silicate melts. *Geochim. Cosmochim. Acta* **68**(4), 867–880.

Roy-Barman M. and Allègre C. J. (1994) $^{187}Os/^{186}Os$ ratios of mid-ocean ridge basalts and abyssal peridotites. *Geochim. Cosmochim. Acta* **58**(22), 5043–5054.

Roy-Barman M., Wasserburg G. J., Papanastassiou D. A. and Chaussidon M. (1998) Osmium isotopic compositions and Re–Os concentrations in sulfide globules from basaltic glasses. *Earth Planet. Sci. Lett.* **154**, 331–347.

Santos J. F., Schärer U., Gil Ibarguchi J. I. and Girardeau J. (2002) Genesis of pyroxenite-rich peridotite at cabo ortegal (NW Spain): geochemical and Pb–Sr–Nd isotope data. *J. Petrol.* **43**(1), 17–43.

Sattari P., Brenan J. M., Horn I. and McDonough W. F. (2002) Experimental constraints on the sulfide- and chromite-silicate melt partitioning behavior of rhenium and platinum-group elements. *Econ. Geol.* **97**, 385–398.

Schaltegger U., Desmurs L., Manatschal G., Müntener O., Meier M., Frank M. and Bernoulli D. (2002) The transition from rifting to sea-floor spreading within a magma-poor rifted margin: field and isotopic constraints. *Terra Nova* **14**, 156–162.

Scherstén A., Elliott T., Hawkesworth C. J. and Norman M. (2004) Tungsten isotope evidence that mantle plumes contain no contribution from the Earth's core. *Nature* **427**, 234–237.

Schiano P., Birck J.-L. and Allègre C. J. (1997) Osmium–strontium–neodymium–lead isotopic covariations in mid-ocean ridge basalt glasses and the heterogeneity of the upper mantle. *Earth Planet. Sci. Lett.* **150**, 363–379.

Schmid S. M., Fügenschuh B., Kissling E. and Schuster R. (2004) Tectonic map and overall architecture of the Alpine orogen. *Eclogae Geol. Helv.* **97**, 93–117.

Shaw D. M. (1970) Trace element fractionation during anatexis. *Geochim. Cosmochim. Acta* **34**, 237–243.

Shirey S. B. and Walker R. J. (1998) The Re–Os isotope system in cosmochemistry and high-temperature geochemistry. *Annu. Rev. Earth Planet. Sci.* **26**, 423–500.

Sinigoi S., Comin-Chiaramonti P., Demarchi G. and Siena F. (1983) Differentiation of partial melts in the mantle: evidence from the Balmuccia peridotite, Italy. *Contrib. Mineral. Petrol.* **82**, 351–359.

Sobolev A. V., Hofmann A. W., Sobolev S. V. and Nikogosian I. K. (2005) An olivine-free mantle source of Hawaiian shield basalts. *Nature* **434**, 590–597.

Stampfli G. M. and Borel G. D. (2004) The TRANSMED transects in space and time: constraints on the paleotectonic evolution of the mediterranean domain. In *The TRANSMED Atlas* (ed. W. Cavazza). Springer-Verlag, pp. 54–90.

Suen C. J. and Frey F. A. (1987) Origins of the mafic and ultramafic in the Ronda peridotite. *Earth Planet. Sci. Lett.* **85**, 183–202.

Takahashi N. (1992) Evidence for melt segregation towards fractures in the Horoman mantle peridotite complex. *Nature* **359**, 52–55.

Takazawa E., Frey F. A., Shimizu N., Saal A. E. and Obata M. (1999) Polybaric petrogenesis of mafic layers in the horoman peridotite complex, Japan. *J. Petrol.* **40**(12), 1827–1851.

van Acken D., Becker H. and Walker R. J. (2008) Refertilization of Jurassic oceanic peridotites from the Tethys Ocean – implications for the Re–Os systematics of the upper mantle. *Earth Planet. Sci. Lett.* **268**, 171–181.

Van Orman J. A., Keshav S. and Fei Y. (2008) High-pressure solid/liquid partitioning of Os, Re and Pt in the Fe–S system. *Earth Planet. Sci. Lett.* **274**, 250–257.

Vaselli G., Downes H., Thirlwall M. F., Dobosi G., Coradossi N., Seghedi I., Szakacs A. and Vannucci R. (1995) Ultramafic xenoliths in plio-pleistocene alkali basalts from the eastern Transylvanian basin: depleted mantle enriched by vein metasomatism. *J. Petrol.* **36**(1), 23–53.

Voshage H., Sinigoi S., Mazzuchelli M., Demarchi G., Rivalenti G. and Hofmann A. W. (1988) Isotopic constraints on the origin of ultramafic and mafic dikes in the Balmuccia peridotite (Ivrea Zone). *Contrib. Mineral. Petrol.* **100**, 261–267.

Walker R. J., Carlson R. W., Shirey S. B. and Boyd F. R. (1989) Os, Sr, Nd, and Pb isotope systematics of southern African peridotite xenoliths: implications for the chemical evolution of

subcontinental mantle. *Geochim. Cosmochim. Acta* **53**, 1583–1595.

Walker R. J., Morgan J. W., Horan M. F., Czamanske G. K., Krogstad E. J., Fedorenko V. A. and Kunilov V. E. (1994) Re–Os isotopic evidence for an enriched mantle source for the Noril'sk-type, ore-bearing intrusions, Siberia. *Geochim. Cosmochim. Acta* **58**(19), 4179–4197.

Walker R. J., Morgan J. W., Beary E. S., Smoliar M. I., Czamanske G. K. and Horan M. F. (1997) Applications of the ^{190}Pt–^{186}Os isotope system to geochemistry and cosmochemistry. *Geochim. Cosmochim. Acta* **61**(22), 4799–4807.

Wallace P. and Carmichael I. S. E. (1992) Sulfur in basaltic magmas. *Geochim. Cosmochim. Acta* **56**, 1863–1874.

Weissert H. and Bernoulli D. (1985) A transform margin in the Mesozoic Tethys: evidence from the Swiss Alps. *Geol. Rundsch.* **74**(3), 665–679.

Wendlandt R. F. (1982) Sulfide saturation of basalt and andesite melts at high pressures and temperatures. *Am. Mineral.* **67**, 877–885.

Xu Y. (2002) Evidence for crustal components in the mantle and constraints on crustal recycling mechanisms: pyroxenite xenoliths from Hannuoba, North China. *Chem. Geol.* **182**, 301–322.

Yasuda A., Fujii T. and Kurita K. (1994) Melting phase relations of an anhydrous mid-ocean ridge basalt from 3 to 20 GPa: implications for the behavior of subducted oceanic crust in the mantle. *J. Geophys. Res.* **99**(B5), 9401–9414.

Yaxley G. M. and Green D. H. (1998) Reactions between eclogite and peridotite: mantle refertilisation by subduction of oceanic crust. *Schweiz. Mineral. Petrogr. Mitt.* **78**, 243–255.

Associate editor: Mark Rehkamper